THESIS FOR THE DEGREE OF DOCTOR OF PHILOSOPHY IN SOLID AND STRUCTURAL MECHANICS

Transition zone design for reduced track settlements − Field measurements and numerical simulations

KOUROSH NASROLLAHI

Department of Mechanics and Maritime Sciences
Division of Dynamics
CHALMERS UNIVERSITY OF TECHNOLOGY
Gothenburg, Sweden, 2025

Transition zone design for reduced track settlements − Field measurements and numerical simulations
KOUROSH NASROLLAHI
ISBN 978-91-8103-268-0

Doktorsavhandlingar vid Chalmers tekniska högskola
Ny serie nr. 5726
ISSN ISSN0346-718X
Department of Mechanics and Maritime Sciences
Division of Dynamics
Chalmers University of Technology
SE-412 96 Gothenburg, Sweden
Telephone + 46 (0)31-772 1000

Cover:

An overview of the instrumented transition zone between ballasted track and 3MB slab track at Gransjö, north of Boden, Sweden.

Chalmers Reproservice

Gothenburg, Sweden 2025

Transition zone design for reduced track settlements − Field measurements and numerical simulations

KOUROSH NASROLLAHI
Department of Mechanics and Maritime Sciences
Chalmers University of Technology

ABSTRACT

In a transition zone between two different railway track forms, the discontinuity in structural design leads to a gradient in track stiffness. This gradient, combined with differences in loading and support conditions along the interface between superstructure and substructure on either side of the transition, often leads to differential settlement and irregularities in vertical track geometry shortly after construction due to ballast densification, subsoil compaction and consolidation. These irregularities amplify dynamic traffic loads, exacerbating long-term track degradation due to differential settlement along the transition zone.

The research in this thesis aims to enhance the understanding of vehicle–track–soil dynamic interactions and the mechanisms driving differential settlement in transition zones, ultimately supporting improved track design and management strategies. A comprehensive suite of numerical models has been developed, including both linear and nonlinear two-dimensional (2D) and three-dimensional (3D) finite element (FE) models of ballasted track, a 2D slab track model, a 2D vehicle model, and a coupled 3D FEM–discrete element method (DEM) model.

The model of short-term dynamic vehicle–track interaction in the time domain provides sleeper–ballast contact forces that are used in an empirical model of long-term settlement, which is used as input in the next simulation of dynamics, etc. Using this iterative approach, these models effectively simulate long-term differential settlement in the ballast and subgrade layers, capturing key phenomena such as sleeper voiding, rail seat load redistribution, and the evolution of vertical track geometry irregularities near transitions. In contrast, the integrated FEM–DEM approach directly computes dynamic responses and long-term differential settlements without relying on empirical settlement models.

Using this iterative methodology to analyse various scenarios, including transitions between ballasted track and 3MB slab track under heavy haul traffic, and transitions from ballasted track to slab track in tunnels, the analyses address stiffness gradients, variability in track support, rail level misalignments, and ballast particle rearrangements induced by dynamic loads. Further, transition zone designs, such as with the use of under sleeper pads, rail pads with different stiffness, transition wedges, wider sleeper bases, and reduced sleeper spacing, are evaluated.

In parallel, an advanced monitoring setup, employing fibre Bragg grating sensors, was developed and deployed for long-term, in-situ measurement of track bed degradation under harsh environmental conditions. The instrumentation included optical strain gauges, accelerometers, and displacement transducers, supported by geotechnical site investigations and total station measurements. This comprehensive set of field test data has been key for model verification and calibration.

Keywords: Transition zone, dynamic vehicle–track interaction, non-linear track model, fibre Bragg grating sensors, condition monitoring, differential settlement, reduced order model

PREFACE AND ACKNOWLEDGEMENTS

The research presented in this thesis was conducted between October 2020 and October 2025 at the Division of Dynamics, Department of Mechanics and Maritime Sciences, Chalmers University of Technology. It was performed as part of the activities within the National Centre of Excellence in Railway Mechanics, CHARMEC (CHAlmers Railway MEChanics, see www.charmec.chalmers.se), in the project TS22 – *Transition zone design for reduced track settlements*.

The study received partial funding from the European Union's Horizon 2020 research and innovation programme, through the projects In2Track2 and In2Track3 (grant agreement Nos. 826255 and 101012456), and from Europe's Rail Flagship Project IAM4RAIL – Holistic (grant agreement No. 101101966). CHARMEC's industrial partners have supported the project. In particular, the support from Trafikverket is gratefully acknowledged. Parts of the computations were enabled by resources provided by Chalmers e-Commons at Chalmers.

I would like to express my sincere gratitude to my main supervisor, Professor Jens Nielsen, for introducing me to the field of railway dynamics, for your support, and for giving me the opportunity to grow as a researcher and a person. Your willingness to help, whether through thoughtful discussions, advice on difficult problems, or careful proofreading, has meant a great deal to me and will leave a lasting influence on my life. I want to thank my co-supervisor, Professor Jelke Dijkstra, for guiding me into the experimental field, for helping me understand how models can be pushed to reflect real-world phenomena, and for your timely encouragement, which often came just when it was most needed. I would like to thank my examiner, Professor Magnus Ekh, for your invaluable expertise in numerical and material modelling, and your support throughout my doctoral studies. I also wish to express my appreciation to my co-authors, Dr Emil Aggestam, Dr Ana Ramos, and Mr Alireza Ahmadi, for the collaboration.

I extend my appreciation to Dr Bruno Zuada Coelho and the team at Deltares in Delft, the Netherlands, for hosting me as a guest researcher during a six-week period in November and December 2024. I am grateful to the measurement campaign team, particularly Mr Anders Karlsson at the Department of Architecture and Civil Engineering at Chalmers, Drs Matthias Asplund and Rikard Granström at Trafikverket, and Mr Carlos Hermosilla at Mammoet, formerly at ACCIONA. Furthermore, I would like to thank the members of the project reference group: Drs Emil Aggestam, Martin Li, Martin Schilke, and Kenneth Viking from Trafikverket, Dr Carl Wersäll from Kerberos Geoteknik, and Professor Stefan Larsson at KTH. Also, I would like to thank Docent Astrid Pieringer and Dr Jannik Theyssen for providing measured data.

I am thankful to my colleagues in the Divisions of Dynamics, Material and Computational Mechanics, Vehicle Safety, and Maritime Technology for the time we have shared. My appreciation also goes out to my friends in Sweden and many dear friends all over the world. Finally, I would like to extend my heartfelt gratitude to my family for their constant encouragement, and to my beloved wife, Nasrin, for her unwavering, boundless, and selfless love, and uplifting support.

Gothenburg, September 2025,

Kourosh Nasrollahi

To a peaceful world, where war has no place.

THESIS

This thesis consists of an extended summary and the following appended papers:

Paper A K. Nasrollahi, J.C.O. Nielsen, E. Aggestam, J. Dijkstra and M. Ekh. Prediction of long-term differential track settlement in a transition zone using an iterative approach. *Engineering Structures*, 2023, 283, 115830. DOI 10.1016/j.engstruct.2023.115830.

Paper B K. Nasrollahi, J. Dijkstra and J.C.O. Nielsen. Towards real-time condition monitoring of a transition zone in a railway structure using fibre Bragg grating sensors. *Transportation Geotechnics*, 2024, 44, 101166. DOI 10.1016/j.trgeo.2023.101166.

Paper C K. Nasrollahi, J.C.O. Nielsen and J. Dijkstra. A review of methods and challenges for monitoring of differential settlement in railway transition zones. *Proceedings of* the *13th International Conference on Structural Health Monitoring of Intelligent Infrastructure* (SHMII-13), 1–5 September 2025, Graz, Austria.

Paper D K. Nasrollahi, A. Ramos, J.C.O. Nielsen, J. Dijkstra and M. Ekh. Benchmark of calibrated 2D and 3D track models for simulation of differential settlement in a transition zone using field measurement data. *Engineering Structures*, 2024, 316, 118555. DOI 10.1016/j.engstruct.2024.118555.

Paper E K. Nasrollahi and J.C.O. Nielsen. Influence of sleeper base area and spacing on long-term differential settlement in a railway track transition zone. *Proceedings of the Sixth International Conference on Railway Technology: Research, Development and Maintenance* (Railway Technology 2024, 1–5 September 2024, Prague, Czech Republic). DOI 10.4203/ccc.7.17.2.

Paper F K. Nasrollahi, J.C.O. Nielsen, and J. Dijkstra. Enhanced three-dimensional reduced-order track model for predicting differential settlement in railway transition zones. Manuscript to be submitted to an international journal.

Paper G A. Ahmadi, K. Nasrollahi, J.C.O. Nielsen and J. Dijkstra. Dynamic vehicle–track interaction and differential settlement in a transition zone on railway ballast: An integrated 3D discrete–continuum model. Manuscript submitted to an international journal.

The appended papers were prepared in collaboration with the co-authors. In Papers A–F, the author of this thesis was primarily responsible for the progress of the work, including participation in planning, developing the theoretical framework and numerical implementation, data processing, instrumenting the test site, conducting measurements, running numerical simulations, and writing the papers. In Paper G, the numerical simulations and manuscript writing were conducted in close collaboration with Mr Alireza Ahmadi, who was responsible for the discrete element modelling.

OTHER PUBLICATIONS BY THE AUTHOR

- A. Ramos, A. Gomes Correia, K. Nasrollahi, J. C. O. Nielsen and R. Calçada. An innovative data-driven hybrid methodology for reliable prediction of rail track deformation. In Proceedings of the 21st International Conference on Soil Mechanics and Geotechnical Engineering (ICSMGE 2026), June 14–19, 2026, Vienna, Austria (submitted manuscript).

- K. Nasrollahi, A. Ramos, J.C.O. Nielsen, J. Dijkstra and M. Ekh. Calibration of 2D and 3D track models for simulation of vehicle–track interaction and differential settlement in transition zones using field-measurement data. *Lecture Notes in Mechanical Engineering*, 2025, 711–720. DOI 10.1007/978-3-031-66971-2_74.

- A. Ramos, A. Gomes Correia, K. Nasrollahi, J.C.O. Nielsen and R. Calçada. Machine-learning models for predicting permanent deformation in railway tracks. *Transportation Geotechnics*, 2024, 47, 101289. DOI 10.1016/j.trgeo.2024.101289.

- K. Nasrollahi. Differential railway track settlement in a transition zone – Field measurements and numerical simulations. Licentiate thesis, Department of Mechanics and Maritime Sciences, Chalmers University of Technology, Gothenburg, Sweden, 2023.

- K. Nasrollahi, J. Dijkstra, J.C.O. Nielsen and M. Ekh. Long-term monitoring of settlements below a transition zone in a railway structure. *Proceedings of the 11th International Symposium on Field Monitoring in Geomechanics* (ISFMG 2022, 4–7 September 2022, London, United Kingdom).

- K. Nasrollahi, J.C.O. Nielsen, E. Aggestam, J. Dijkstra and M. Ekh. Prediction of differential track settlement in transition zones using a non-linear track model. *Advances in Dynamics of Vehicles on Roads and Tracks II: Proceedings of the 27th Symposium of the International Association of Vehicle System Dynamics* (IAVSD 2021, 17–19 August 2021, Saint Petersburg, Russia).

CONTENTS

PART I – EXTENDED SUMMARY

1 Introduction

1.1 Background and motivation

Railways are a sustainable, cost-effective, and efficient mode of transportation, offering safe and reliable transit for both passengers and goods. They can move large volumes of freight and people over long distances with lower carbon emissions than other modes of transport. Therefore, railway networks play a crucial role in global transportation [1].

In a transition zone between two different railway track forms, there is a discontinuity in track structure leading to a gradient in track stiffness. Examples include transitions between different superstructures, e.g., slab track to ballasted track, and/or between different substructures, e.g., embankment to a bridge or tunnel structure. Differences in loading and support conditions at the interfaces between the track superstructure and substructure on either side of the transition often lead to differential track settlement and irregularities in longitudinal rail level soon after construction, due to densification of ballast and consolidation of the subgrade. This results in an amplification of the dynamic traffic loading along the transition, contributing to the degradation process of the foundation and resulting in a further deterioration of vertical track geometry [2–20].

To ensure uninterrupted traffic flow, the financial burden associated with addressing issues in railway transition zones can be significant [21,22]. For instance, the annual expenditure on maintenance in U.S. railways is estimated at approximately $200 million [6], whereas the cost in Europe is around $85 million [5]. Transition zones deteriorate at rates up to four to eight times faster than open track, significantly increasing life cycle costs [23]. Consequently, implementing engineered solutions alongside a comprehensive maintenance strategy is essential for ensuring the long-term serviceability of transition zones. This shift from reactive to proactive maintenance requires the capability to model conditions over time. However, such maintenance can be costly and may temporarily reduce network capacity. By understanding the mechanisms behind accelerated track degradation in transition zones, significant improvements can be achieved in the design of new railway structures and in the proactive maintenance of existing ones as networks modernise and capacity demands increase.

Railway networks are particularly compared to other modes of transportation vulnerable to climate and natural hazards, including high temperatures, heatwaves, heavy rainfall, snowfall, earthquakes, flooding, and extreme winds, due to their linear and exposed nature. Conventionally designed in accordance with historical climate patterns and recognized risks, numerous rail systems are presently encountering operational thresholds that are being repeatedly exceeded. This has resulted in structural failures, service disruptions, and increased lifecycle costs. The adverse impacts of climate hazards are extensive, including but not limited to track buckling [24,25], landslides, flooding, washouts, operational delays, and heightened maintenance demands. These effects undermine availability, punctuality, and safety, while

significantly increasing operational and maintenance costs. For instance, within the Swedish railway network, climate-related events have been shown to account for 5 to 10 percent of total failures and up to 60 percent of service interruptions [26]. In countries such as Sweden, where the climate is characterized by cold winters and relatively warm summers, climate change poses additional challenges to railway infrastructure. Addressing these challenges requires enhancing the resilience of railways while also meeting the growing demand to accommodate greater loads, such as high-speed operations, and higher traffic intensities, such as increased train frequency. A better understanding of these factors can support significant improvements in the design of new railway structures, particularly across the European countries. Although this aspect is not examined in the present thesis, it could serve as a valuable direction for future research.

1.2 Aim of research

The objectives of this research are two-fold: first, to develop a methodology for assessing and quantifying the long-term performance of transition zones between different track forms by simulation or field measurements; and second, to provide design guidelines for improving transition zone performance. To this end, the following parts have been completed and are presented in this thesis.

- Development of simulation models for predicting long-term differential track settlement in transition zones using an iterative approach (**Paper A**), including refinement and calibration of a two-dimensional (2D) track model by considering sleeper coupling via the ground (**Paper D**)
- Real-time condition monitoring of an in-situ transition zone using fibre Bragg grating sensors (**Paper B**), with the measured data later used to verify and calibrate the model (**Paper D**).
- Numerical studies into the effects of sleeper base area and spacing, under sleeper pads, softer rail pads, and transition wedges on long-term differential settlement in railway transition zones using the developed models (**Papers A, E-F**).
- Development of an enhanced 3D reduced-order track model for predicting differential settlement in railway transition zones, incorporating the variation in static stiffness of the substructure along the transition zone (**Paper F**), to enable the modelling of transition zone designs in the substructure
- Analysis of dynamic vehicle–track interaction and differential settlement in a railway ballast transition zone using an integrated 3D discrete–continuum model, enabling prediction of the initial phase of differential settlement without reliance on empirical settlement models (**Paper G**).
- Numerical studies on the influence of various irregularities, including variations in support conditions, stiffness gradients, and initial misalignment at rail level (**Papers A, F-G**).

- Development of a threshold-based empirical settlement model and subsequent calibration of parameters against field measurements to predict long-term settlement in the ballast layers (**Papers A-F**). Additionally, an empirical settlement model to estimate long-term settlement in the subgrade layers has been implemented (**Paper F**).

1.3 Scope

The work in this thesis has been conducted as part of a multidisciplinary research project that integrates numerical modelling with field measurements. It includes an extensive field-testing campaign and long-term condition monitoring of a transition zone at the Gransjö demonstrator site on the Malmbanan line, as part of the EU project In2Track3, which was part of the European Union's Horizon 2020 research and innovation programme Shift2Rail.

Some of the challenges included the difficulties in performing field measurements for data acquisition in the harsh environmental conditions at the test site, such as the wide temperature range and freeze-thaw cycles in northern Sweden, which can affect both the condition monitoring equipment and the long-term behaviour of the track and subgrade. Another difficulty was the operational variability in train types and axle loads.

Additionally, the project encompasses numerical modelling of geotechnical behaviour and dynamic vehicle–track interaction, alongside extensive data post-processing. The primary objective of this project is to develop tools for predicting long-term differential track settlement in railway transition zones. These tools can consider different transition zone designs with varying levels of complexity in the models. Each approach necessitates assumptions and simplifications to attain an acceptable level of accuracy at a reasonable cost for sensors, test equipment and computational effort.

Overall, this thesis aims to advance the understanding of dynamic interactions between vehicles and track, as well as between the track and the underlying soil, while investigating the mechanisms that contribute to differential settlement in transition zones.

1.4 Limitations

To limit the scope of the thesis, the research has been subjected to the following limitations:

- Lateral dynamic effects are not included in the modelling.
- The performance of transition zones in curves is not investigated, as this would require a more extensive 3D model.
- The influence of wave propagation and the dynamics of the subgrade is not fully considered in the 2D models. A more advanced model of the foundation would be required if vehicle speeds approach the fundamental wave speed of the subgrade.
- Settlement on the track side adjacent to the engineering structure is not examined (although it could be considered in future work using the models developed in this thesis).

- Empirical models that consider a combination of deterioration mechanisms are employed; however, the physics of individual mechanisms, such as ballast breakage and fouling, and their respective contributions to accumulated deterioration, are not modelled in detail.

2 Transition zones

2.1 Components

In general terms, a transition zone consists of three parts: a so-called open track on ballast, an approaching zone either on ballast or on another type of engineering structure, and the engineering structure itself, see the example in Figure 2.1. The open track is relatively far away and therefore unaffected by the presence of the engineering structure. The general recommendation used by the Swedish Transportation Administration is that the length of the transition zone (approaching zone in Figure 2.1) should be at least the distance the vehicle travels during half of a second [27]. Typical lengths of transition zones are 5 – 30 metres in literature [28]. The approaching zone is located close to the engineering structure and may suffer from severe track degradation and differential settlement in the case of a poorly performing design. The engineering structure can be a bridge, culvert, tunnel, or a level crossing. In this thesis, the transition is between a ballasted track and a ballastless/slab track, or a bridge and a tunnel see Figure 2.2.

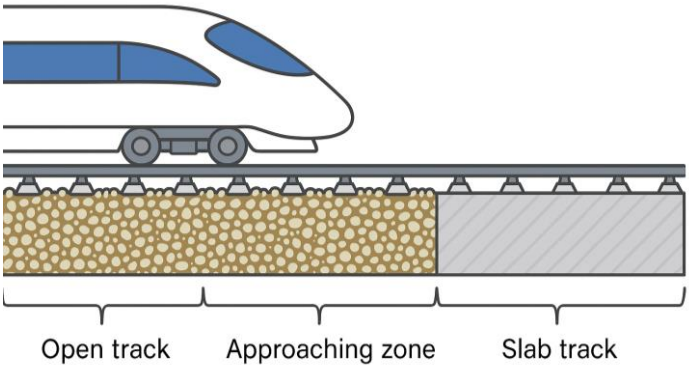

Figure 2.1: Schematic diagram of the different parts of a transition zone.

An example of a layout of the transition zone between ballasted track and slab track is presented in Figure 2.3(a). The ballasted track includes several layers of geomaterials to safely transmit and distribute the train-induced load into the subgrade. It comprises a superstructure and a substructure. The superstructure consists of the rails, sleepers, rail pads, rail fastening systems and sometimes under sleeper pads (USP). The substructure includes geotechnical layers such as the ballast, sub-ballast, backfill and subgrade, whose characteristics significantly influence the track response [29], see Figure 2.3(b).

Traditionally, the layers of the substructure are designed using empirical and simplified theoretical approaches based on experience from in-service tracks, augmented with extensive laboratory and field test data [30,31]. However, these conventional design approaches may lack general applicability in different traffic and soil conditions. This serious limitation has become

more apparent with the dramatic increase in transportation needs, which has accelerated the deterioration of existing tracks and incurred significant maintenance costs. Thus, to reach optimum performance of railway tracks, including transition zones, there is an inevitable need for a more reliable, practical, and adaptable design method. The development of such a design technique requires a detailed analysis of the mechanical behaviour of both track superstructure and substructure, as well as their mutual interaction.

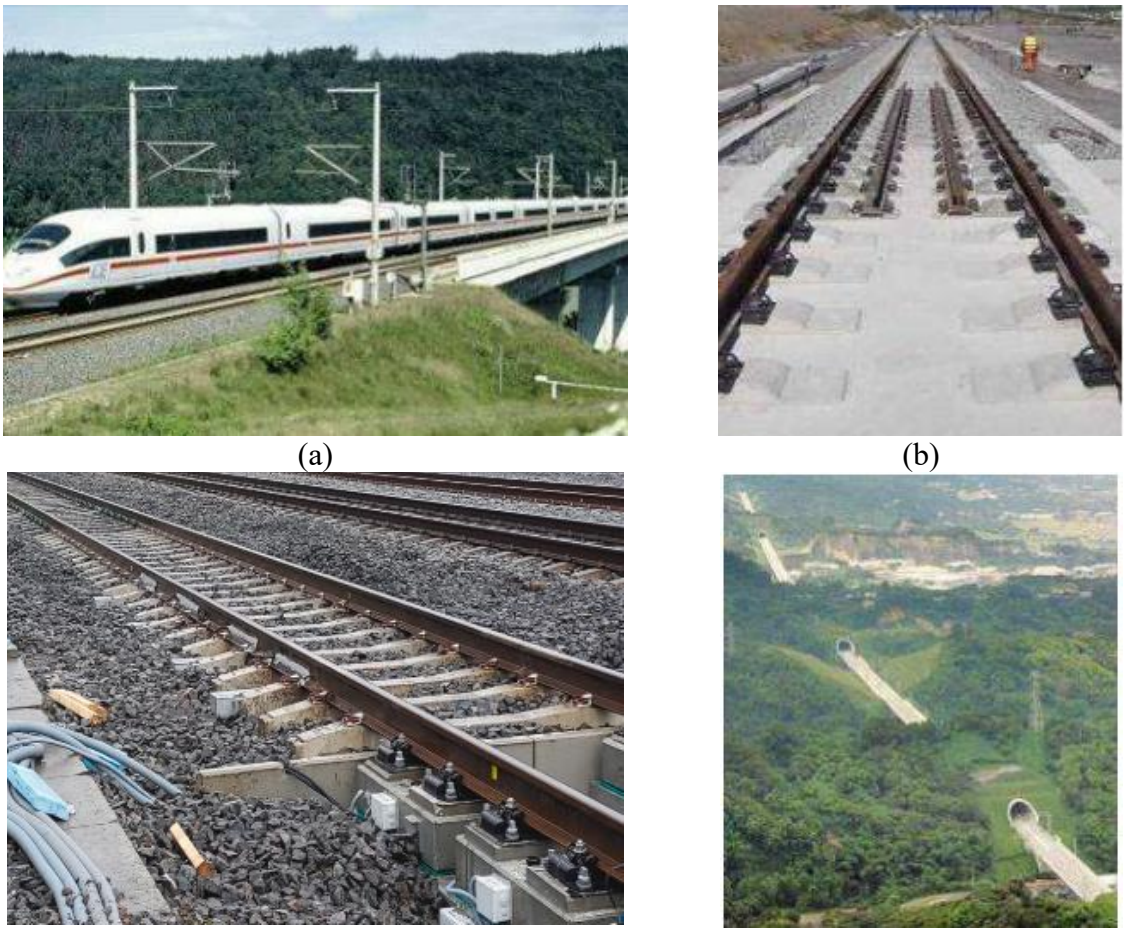

(a) (b) (c) (d)

Figure 2.2. Examples of transition zones: a) between ballasted track on embankment and bridge [32], b) between ballasted track and slab track [32], c) between ballasted track and 3MB slab track at Gransjö, north of Boden, Sweden [9], d) successive transitions between track on bridge and track in tunnel [32].

The high availability and relatively low cost of ballast make it an ideal geomaterial for railway applications. The ballast is formed by a layer of medium to coarse-sized particles (32 – 64 mm) of angular-shaped, uniformly graded granular material, free from dust, and not susceptible to cementation [33], see Figure 2.4. It must facilitate drainage, resist frost action, and allow for adjustments of track geometry. The main function is to distribute the train loads to the underlying subsoil, attenuate dynamic loading, provide lateral resistance, and ensure rapid

drainage [33]. The ballast layer must ensure a uniform distribution of loads to the underlying subgrade, and its optimum thickness is usually 250 – 300 mm measured from the bottom surface of the sleepers [33]. This layer is of paramount importance in railway design, as it endures the highest stress levels in the substructure due to the recurrent loading from numerous wheel passages, making it vulnerable to various forms of degradation that contribute to substantial settlement.

Densification of ballast is the result of particles rearranging and settling into a tighter configuration [34], which closes voids and increases stiffness. This is investigated in **Paper G**. Crushing occurs when individual particles are subjected to stresses exceeding their internal shear strength, leading to fragmentation into smaller particles [7]. Abrasion or surface polishing, caused by repeated sliding, rolling, and low-energy impacts, gradually smooth and round the particles, reducing their interlocking properties and shear resistance [35]. Impact-induced fatigue fracture is the result of a combination of repeated low-amplitude cycles and occasional high-amplitude impacts, such as those caused by wheels with flats or from wheels traversing discrete track irregularities [35]. These impacts initiate micro-cracks that coalesce over time. This process reduces the material's fatigue limit. Freeze–thaw spalling occurs when water infiltrates the micro-pores of ballast grains and subsequently freezes, causing volumetric expansion and generating tensile stresses capable of detaching small flakes from the surface [36]. Furthermore, the generation of fines can lead to ballast fouling when the volume of fines exceeds 15 – 20%, resulting in clogged voids, water entrapment, and impaired drainage.

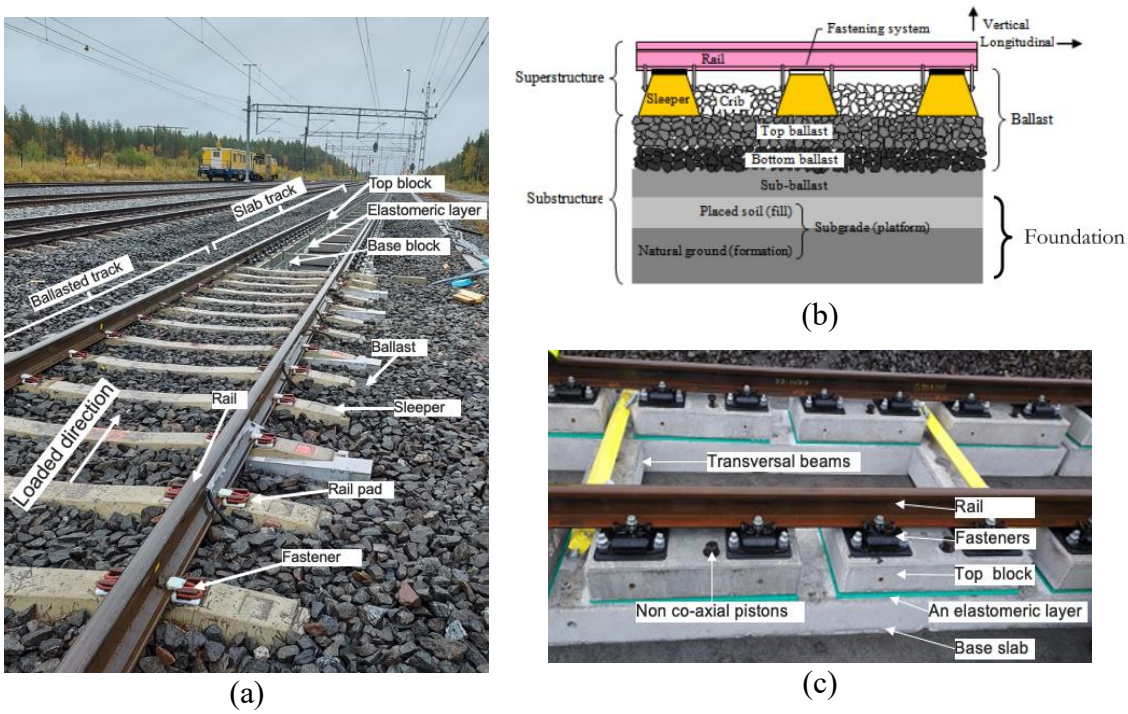

Figure 2.3. (a) View of transition zone between ballasted track and 3MB slab track; (b) Cross-section of ballasted track including rail, rail pads, fasteners, sleepers (crossties), ballast, sub-ballast, and subgrade [30]; (c) 3MB slab track design consisting of base slabs, top blocks, and an elastomeric layer between the concrete layers.

The sub-ballast is the granular layer located between the ballast and the subgrade. Generally, it is placed as a specific layer, but it may also develop over time from particle wear, densification of ballast, or the accumulation of older ballast layers due to decades of loading and track maintenance. In some locations, this can result in sub-ballast layers reaching depths of 0.8 – 1 m [9]. The sub-ballast distributes the load and reduces stress on the subgrade, with its effectiveness depending on its stiffness and thickness. Furthermore, this layer must be well-drained to avoid the buildup of positive pore water pressure under repeated loading. It should consist of durable, angular particles that interlock and resist abrasion, provide separation between the ballast and subgrade, and offer frost protection in cold climates [29,37], see Figure 2.4 for the range of particle sizes of ballast and sub-ballast particles.

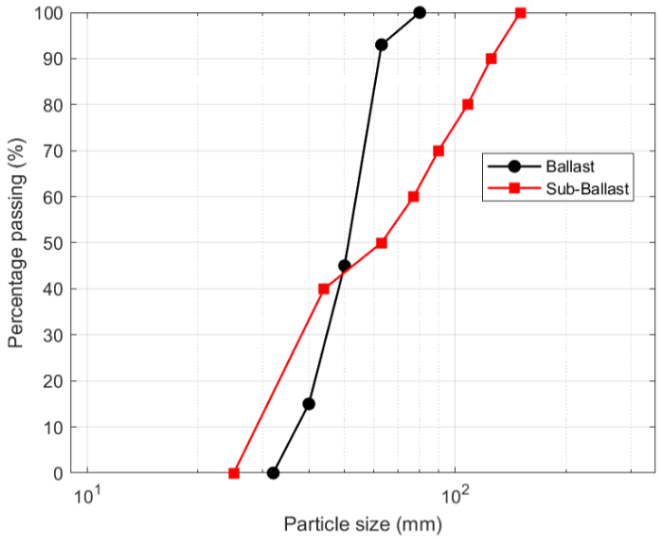

Figure 2.4. Particle size distribution of the granular materials used in **Paper G**.

The subgrade, which serves as the foundation for all overlying track components, is often the most variable and potentially weakest part of the railway structure [29,37]. The primary objective is to establish a stable base for the ballast and sub-ballast layers. The subgrade conditions can vary significantly, depending on the geological setting and the conditions present at the construction site. Consequently, the impact of differential settlement within this layer may be substantial and should be carefully considered, particularly in transition zones where long-term differential settlement can affect track performance. Fine-grained soils exhibit a higher susceptibility to plastic flow under cyclic loading conditions, resulting in a reduction in support stiffness over time. The presence of moisture has been demonstrated to decrease effective stress, soften fine-grained soils, and potentially cause ballast particle migration. Seasonal frost heave is defined as the lifting of the track when water in the subgrade freezes into ice lenses.

Even though ballasted track is the most common track form, modern infrastructure for high-speed railway traffic is often built using slab track [38]. Compared to ballasted track, slab track has several advantages, e.g., higher lateral track resistance and eliminated problems with ballast degradation. This reduces the need for regular maintenance and extends service life. However, should maintenance work on slab track be required, it is often more costly compared to

maintenance work on ballasted track. Furthermore, there is less tolerance for corrections of track geometry compared to ballasted track. Over the years, the use of optimised and prefabricated slab track systems has increased, and the initial cost ratio compared to ballasted track has been reduced [14]. For example, the “Moulded Modular Multi-Blocks slab track” (3MB) concept is a reinforced standard precast slab track designed for both mixed and high-speed traffic [39]. As part of the European Union's Horizon 2020 research and innovation programme in the projects In2Track2 and In2Track3, this particular design was demonstrated in the field on a short section of track on the heavy haul line Malmbanan in Sweden, with tests between autumn 2022 and June 2023.

2.2 Problems in transition zones

The main problems occurring in transition zones are:

- Stiffness gradient between two different track forms leading to higher dynamic loads
- Differential track settlement and the formation of an irregularity in longitudinal rail level due to degradation mechanisms in the substructure

Uneven (differential) settlement is more pronounced in railway transition zones than along open track sections. However, variations in support conditions along open track can also lead to differential settlement, see Figure 2.5. Existing research indicates that the ballasted track section typically experiences greater settlement than the adjacent, stiffer engineered structure. The phenomenon is primarily attributable to long-term plastic deformation in the track-bed layers when subjected to recurrent train loads, combined with creep due to the self-weight of the foundation soils. Differential settlement is often manifested as defects in track geometry, most visibly as irregularities at track level. A discrepancy in settlement rates between the ballasted track and the engineering structure is inevitable, but this issue can be exacerbated by additional factors. The present dissertation specifically investigates differential settlement caused by stress and strain amplification in transition zones at relatively low train speeds with high axle loads.

Problems in transition zones have been addressed extensively in the literature. For example, in the review of experimental testing and modelling of transition zones, Indraratna et al. [4] identified the main reasons for differential settlement as hanging (voided) sleepers within the transition and the difference in track stiffness across the transition. Even a minor gap between a sleeper and its support has been shown to result in an uneven stress distribution among adjacent sleepers and an increase in rail stresses. The resulting increases in dynamic wheel–rail contact forces and in-track stresses accelerate degradation, and the strain-energy amplification in the approach zone grows exponentially as more sleepers lose support. This process contributes to various forms of infrastructure degradation, including rail corrugation and wear, cracked sleepers, loosened fastenings, ballast breakage and fouling. Elevated kinetic energy in the ballast layer has also been shown to amplify particle wear, with elements in close proximity to the transition interface retaining this additional energy for a short duration after the train has passed [23].

Wang and Markine [5] and Nasrollahi et al. in **Paper A** concluded that differential settlement has a greater impact on track degradation than stiffness gradient at the transition between two track forms. Also, in Wang and Markine [5], it has been shown that the dynamic vehicle–track interaction is different depending on the direction of travel, whether the traffic is moving from a softer to a stiffer track form, or vice versa. Similar conclusions were drawn in Refs. [40–45]. Differential settlement also leads to the development of dips and bumps near the transition, which has been investigated by many researchers [46–48], see Figure 2.5(b). For example, in the U.S., it was found that more than 50% of all bridge transitions exhibit dips, with an average depth of 33 mm occurring approximately 5.2 m from the bridge [46]. Even on well-constructed and well-maintained track, the support stiffness can vary from one sleeper to the next [49], see Figure 2.5. High variability in support stiffness along the track leads to higher dynamic loads, which increase with train speed.

Track stiffness must be sufficiently high to resist traffic loads, ensure track stability and bearing capacity, and minimise track deterioration. However, excessive track stiffness can lead to elevated stresses in the track structure, see **Paper F**, contributing to wear and fatigue in track components e.g., rails and fastenings. To achieve a good design and low maintenance cost, it is widely accepted that track stiffness and its variation needs to be kept within a certain range, ideally close to an optimum value [50–53]. Vertical track stiffness at rail level is defined as the ratio of the vertical wheel load applied on the running surface of one rail to the resulting vertical rail displacement at the same position [50]. In [53], an optimum value of vertical track stiffness at rail level of approximately 90 kN/mm was suggested for high-speed lines on ballasted track. A similar recommended value for the vertical dynamic track stiffness is 100 kN/mm, which corresponds to a rail deflection of 1.0 mm under a wheel load of 100 kN.

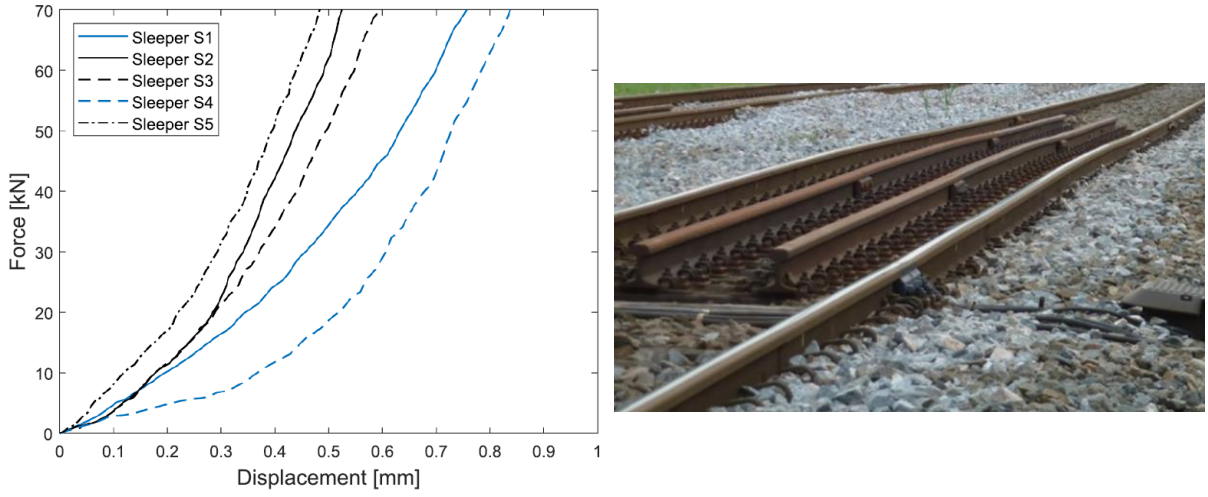

(a) (b)

Figure 2.5. (a) Applied static force versus measured sleeper end displacement for the case with unfastened rails and forces applied symmetrically on the two rail seats of one sleeper, [54]; (b) Transition zone with a large irregularity in longitudinal level due to differential settlement, from [5].

3 Transition zone designs

Reviews of transition zone design can be found in Sañudo et al. [55] and Indraratna et al. [4]. Available solutions to improve transition zones have been categorised in different ways. The main goal of transition zone design is to minimise the difference in track stiffness across the transition between the open track and the engineering structure. By using different distributions and properties of various elements in the superstructure or substructure, it is possible to design an appropriate gradual variation in stiffness along the transition zone. Methods to facilitate such a gradual variation are described in [22]. Sañudo et al. [55] used a categorisation depending on the location of the structure where the design improvement is made. This includes: i) design of the substructure (subgrade), ii) design of the superstructure, and iii) mixed solutions combining i) and ii).

In this thesis, the design solutions related to transition zones are divided into the following four categories, see Sañudo et el. [55]. Several of the solutions are explained in more detail below.

- Mitigation of stiffness gradient in transition zone
- Improved track foundation
- Minimisation of differential long-term vertical displacements between transition and engineering structure
- Combined designs

3.1 Size and spacing of sleepers

For a given bed modulus of the structure below the sleepers, the use of sleepers with larger base area and shorter sleeper spacing will increase track stiffness at rail level. The larger bearing area of the sleeper distributes sleeper–ballast contact forces more evenly over the ballast, reduces stress concentrations and prevents long-term degradation [55,56]. This is investigated in **Paper E**.

3.2 Auxiliary rails

Track stiffness is influenced by the potential implementation and number of auxiliary rails, see Figure 3.1. Although only a limited number of studies have investigated this solution, potential benefits have been demonstrated. For instance, Chumyen et al. [57] concluded that using two auxiliary rails in a transition zone can improve the dynamic characteristics of the track, reduce stiffness gradient and differential track settlement, and enhance stress distribution in the ballasted track. Additionally, placing the auxiliary rails closer to each of the main rails (wider separation) offers slightly better dynamic performance compared to a narrower placement [57]. The dynamic behaviour of a railway transition from slab track to ballasted track, including auxiliary rails, was evaluated using a 3D numerical model for train–track interaction in [18]. The authors concluded that using two auxiliary rails resulted in lower rail deflection variations

across different train speeds. However, adding more than two auxiliary rails provided minimal improvement and is therefore not recommended. In the studies discussed above, auxiliary rails were only added to the softer track side, increasing the stiffness at rail level. However, the study in [58] extended the auxiliary rails to the stiffer side and concluded that the additional rail had less influence on the stiffness gradient. This aspect warrants further investigation in future research. However, the presence of auxiliary rails complicates tamping maintenance operations. Additionally, additional fastening systems and sleepers adapted specifically for auxiliary rails are required.

Figure 3.1. Transition zone with auxiliary rails and a large differential settlement, from [5].

3.3 Rail pads, under sleeper pads, and ballast mats

Rail pads, see Figure 3.2(a), are placed between the rail and the sleeper. The use of soft rail pads reduces the transmission of high-frequency vibrations caused by wheel impacts to the ground and is the most direct method to reduce track stiffness at rail level and distribute traffic loads [8] and **Paper A**. USPs are placed between sleepers and ballast, see Figure 3.2(b). The use of USPs pads is investigated in [59–61]. It provides additional damping, minimises breakage and cracked sleepers, reduces loads between ballast particles and concrete sleepers, reduces ballast degradation, and improves passenger comfort [40,59,62,63]. Low stiffness USPs reduce forces acting on the substructure by extending the load distribution along the track. Ballast mats serve a similar purpose as USPs, see Figure 3.2(c), but due to the load distribution within the ballast layer, they must have significantly higher flexibility to noticeably affect the overall track stiffness, see **Paper A**. Ballast mats [64] are mainly used to reduce ballast degradation and to isolate high-frequency vibrations on bridges. Although these mats and pads are not directly exposed to weather, their maintenance is not straightforward. Additionally, they must withstand the abrasive action of ballast, necessitating the use of durable materials with a long service life.

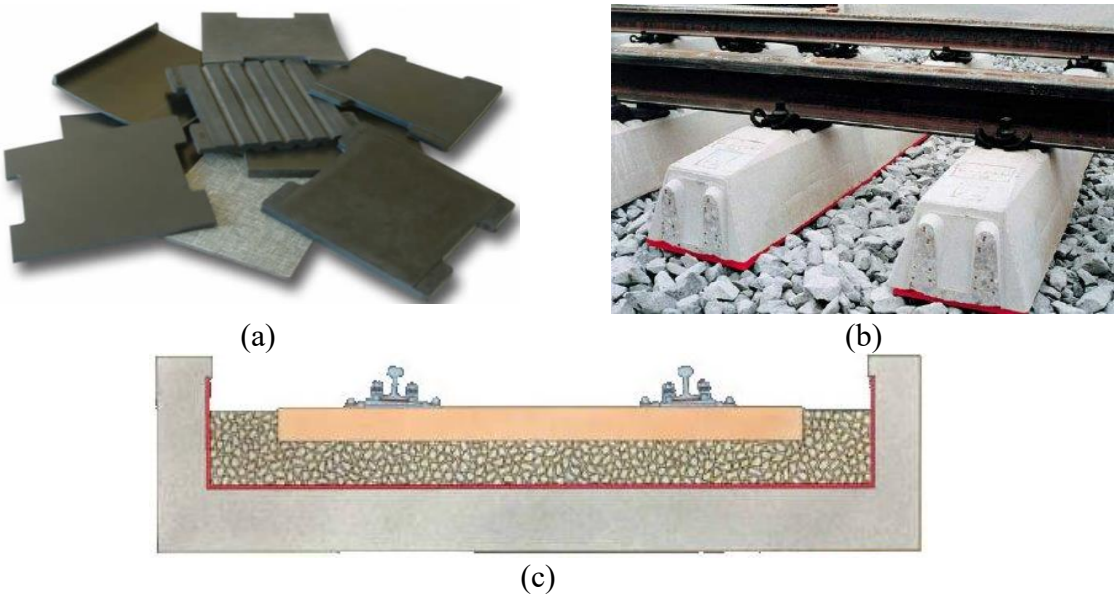

(a) (b)

(c)

Figure 3.2. (a) Rail pads, (b) under sleeper pads [55], and (c) ballast mat [64].

3.4 Sleeper material

Sleepers made of composite material, plastic material, or rubber have been found to be effective in reducing the vertical track stiffness [46,65]. Nicks [46] studied the effect of using wooden, concrete, or plastic sleepers on the dynamic response of a bridge approach and found that wooden sleepers help to mitigate the bumps and dips better than the other materials. However, it was also found that the pressure on ballast and subgrade layers is higher beneath wooden sleepers than beneath concrete sleepers. The effectiveness of various sleeper materials in reducing track stiffness of ballasted track at the transition to a bridge was investigated by Sasaoka et al. [62]. In their study, two methods were tested to smooth the gradient stiffness at an embankment to bridge transition: (1) replacing concrete sleepers with composite (plastic) sleepers, and (2) installing concrete sleepers on the bridge deck with thick rubber pads at the bottom surface of the sleepers. Measurements of vertical track stiffness on the approach to, and on the decks of, bridges with three examined sleeper types (concrete, composite, and concrete with under sleeper pads) were compared. It was found that both the composite sleepers and the concrete sleepers with rubber pads were successful in reducing the track stiffness measured on the approach to the bridge and the vertical track stiffness measured on the bridge.

3.5 Wedge-shaped self-levelling railway sleeper

The operational principle of a wedge sleeper relies on the migration of crib and shoulder ballast into the gap between the sleeper and the underlying ballast. This process is driven by gravitational forces and dynamic vibrations induced by passing trains [66]. This migration serves to mitigate the occurrence of hanging sleepers, as illustrated in Figure 3.3(a). The wedge

shape autonomously promotes ballast migration, and its effectiveness is related to the angle of repose of ballast, as illustrated in Figure 3.3(a). In [67], a series of scaled laboratory tests were conducted to investigate the performance of different wedge geometries. The tests compared a single long wedge to multiple mini wedges, see Figure 3.3(b). Furthermore, 3D DEM simulations were conducted to analyse contact forces within the ballast for different wedge designs. This was followed by 2D DEM simulations to study settlement behaviour. The primary conclusions of this study indicated that the utilisation of a singular, elongated wedge is preferable to the deployment of multiple, smaller wedges. In circumstances where the wedge sleeper angle exceeds the ballast's angle of repose, particles can migrate into voids induced by settlement. Additionally, an augmented wedge sleeper angle promotes enhanced particle migration, thereby optimising sleeper support. However, an extended wedge results in a decrease in the effective ballast height beneath the sleeper, which may impede the retrofitting process on existing lines.

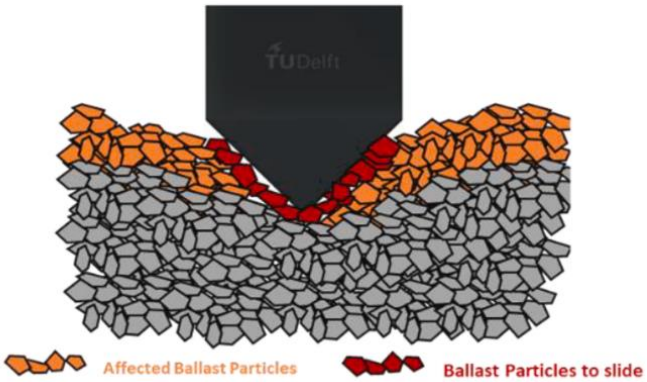

(a)

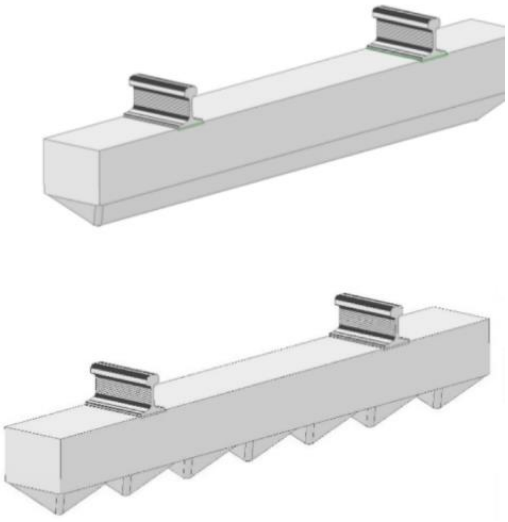

(b)

Figure 3.3. (a) Void correction concept using wedge sleeper, (b) wedge-sleeper designs with a single wedge or multiple wedges. From [67].

3.6 Geocells, soil cement and cement gravel

Geocells are honeycomb-like cellular structures formed by interconnected joints, creating a cellular network used for the confinement and stabilisation of soils. The purpose of using this technique is to reduce the risk of ballast spatter (which especially increases in transition zones) and to minimise differential settlement [68]. They greatly improve track performance by increasing soil stability and track stiffness, see Figure 3.4.

Figure 3.4. Use of geocells in railways [68].

3.7 Soil treatment, polyurethane grout technology and glued ballast

Polyurethane grout is a polymer-based material injected into the ground or a structure to improve their mechanical properties. This technology can be applied to address surface and cross-level track geometry issues caused by ballast layer degradation [69]. Jing et al. [69] reported on the application of polyurethane in transition zones, where it was used to glue ballast particles, enabling a smoother and gradual variation in track stiffness. This resulted in reduced vibration and improved performance within the transition area. The application of glued ballast is illustrated in Figure 3.5. Although track alignment can still be corrected through tamping, this procedure necessitates reapplying glue to the ballast aggregate afterwards. In [70], both experimental testing and numerical simulations demonstrated that epoxy asphalt tracks reduce vertical displacement and vertical stress at the top of the rail and within the surface layer.

Figure 3.5. Glued ballast [71].

3.8 Hot mix asphalt under ballast in track bed layers

A layer of hot mix asphalt placed beneath the ballast reinforces weak subgrade conditions, see Figure 3.6. The preferred asphalt mix is a low- to medium-modulus (plastic) formulation, designed with air voids of 1 to 3 percent, that will easily compact in place to less than 5 percent air voids. This has been achieved by specifying a local dense-graded base mix with a maximum aggregate size of 25 – 38 mm and increasing the asphalt binder content by about 0.5 percent [72]. The solution has been shown to reduce stresses in the subgrade and increase its load-bearing capacity. In addition, it can increase vertical track stiffness, extend track life, and improve track drainage [71].

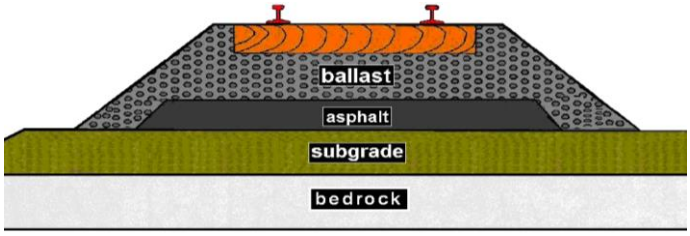

(a)

(b)

Figure 3.6. (a) A sketch of asphalt underlayment without granular sub-ballast, from [71], (b) 30 m of HMA placed at two ends of a Bridgeport, Alabama (USA), bridge approach, from [72].

3.9 Reinforced foundations by piles and stone columns

In soil reinforcement techniques, various elements, such as stone, concrete, or geosynthetics, are inserted to improve the properties of in-situ weak soils. A review of technologies aimed at mitigating problems in transition zones is presented in [68]. These methods include stone columns, compacted columns, driven columns, geopiers, deep soil mixing (involving grout injection through augers that mix in with the soil, forming in-place soil-cement columns), concrete-injected columns, and continuous flight auger cast piles. Using piles or stone columns, see Figure 3.7, increase support stiffness and reduce deformation, resulting in almost zero settlement of the foundation. However, these systems are costly and require heavy machinery for installation [55].

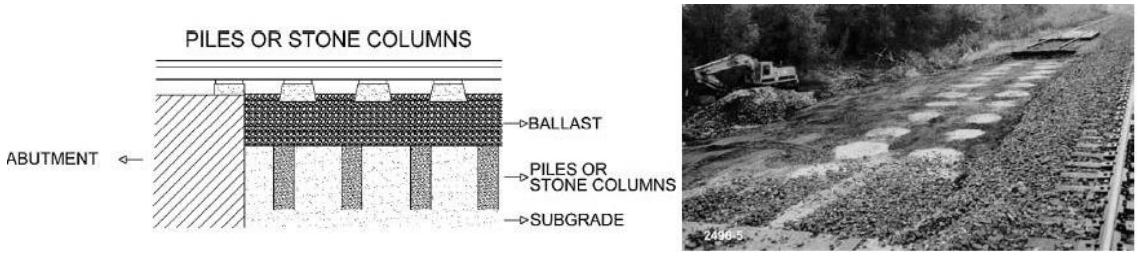

(a) (b)

Figure 3.7. (a) Piles concept solution in a transition zone, and (b) stone columns installed in the subgrade [55].

3.10 Steel slag ballast particle

Steel furnace slag (FS) is a by-product of steel manufacturing, generated during the separation of molten steel. In China, the annual production of FS is estimated at approximately 70 million tonnes [73]. The behaviour of furnace slag-ballast composites (FS-BCs) has been evaluated through shear strength tests, Los Angeles Abrasion (LAA) tests, and plate load tests. Additionally, a field-validated FEM model has been employed to study the dynamic performance of bridge transition zones incorporating FS ballast [73]. The findings indicate that the implementation of FS ballast enhances both the shear strength and bending modulus of the ballast layer. FEM simulations have indicated that increasing the flexural strength ratio reduces rail deflections, thereby improving the performance of bridge transitions.

The LAA test, involving 500 rotations at a frequency of 32 r/min, is a widely employed method for evaluating the toughness and abrasion resistance of granular materials. Suitable ballast must demonstrate resistance to crushing and degradation in order to perform effectively under train loads and to ensure proper load transfer to underlying layers. Mechanical properties, such as shear strength and internal friction angle, can be obtained from direct shear tests. The stiffness of ballast is typically derived from plate load tests. However, it is imperative to acknowledge the sensitivity of plate load tests to test conditions [73].

3.11 Embedded bridge structures

Approach slabs are usually reinforced concrete beams, which may be installed horizontally or with an incline, see Figure 3.8. With this technique, the depth of the ballast is gradually reduced on the approach to the engineering structure. As concluded in [2,74], the effectiveness of this solution relies on the fact that both dynamic track movements and long-term settlements are mainly governed by the depth of the ballast, i.e., the contribution of the subgrade to the overall track stiffness and settlement is of minor importance. For sites with soft subgrade, this design method can smooth the stiffness gradient in a transition zone [75]. However, over time, the inclination of the buried slab may increase due to long-term degradation and settlement of the embankment and subgrade.

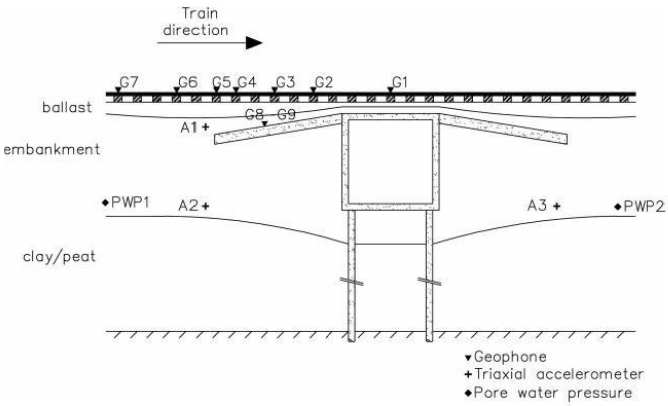

Figure 3.8. Typical section of an inclined approach slab. From [2].

3.12 Transition wedges and ballast settlement ramps

Transition wedges are gradual transitions (typically around 20 m in length), in which the backfill material changes progressively from softer to stiffer, using a bed of (bound or unbound) granular materials and aggregates, see Figure 3.9, [76]. Differential settlement in a transition zone can be reduced and the gradual transition of vertical stiffness between the two structures can be smoother. However, the wedge shape fill materials and construction process must meet strict performance requirements, as the consequences of any malfunction will lead to high repair costs as well as traffic disruptions. An extensive investigation of various transition wedge designs was presented in [16], including single (or inverted) trapezoidal and double trapezoidal shapes with varying inclinations. These configurations increase rail-level track stiffness on the softer side, thereby reducing the stiffness gradient across the transition. As a result, load distribution becomes more uniform, sleeper–ballast contact forces increase, and subgrade settlement is reduced. This system is particularly suitable for areas with soft subgrades.

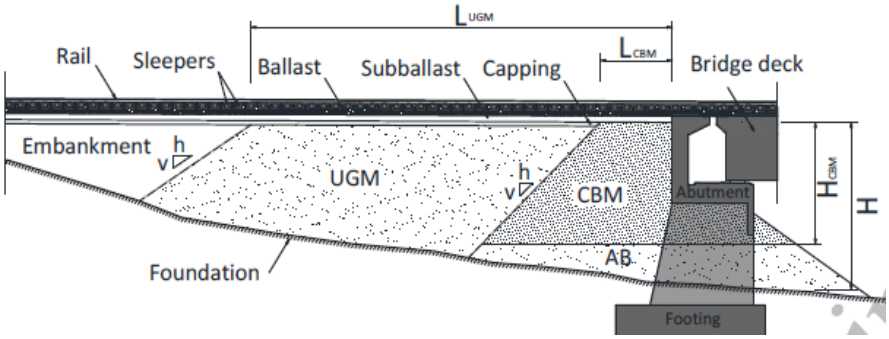

Figure 3.9. Sketch of transition zone design with wedge-shaped backfill. The backfill consists of a wedge with layers of Cement Bound Granular mixtures (CBM), a wedge with layers of Unbound Granular Material (UGM), and an Abutment Backfill base (AB) under the wedge-shaped CBM [32].

3.13 Safe Hull-Inspired Energy Limiting Design (SHIELD)

SHIELD represents a hull-inspired, energy-limiting approach that shares conceptual similarities with transition wedge designs [74], see Figure 3.10. The distinguishing feature of this approach is the optimised geometry, which facilitates the dissipation of energy during the transition from soft to stiff regions, and vice versa. This design has been shown to improve stress distribution along the transition and to reduce the stiffness gradient, resulting in lower vertical acceleration in the lower subgrade layers. However, the long-term influence and the applicability of the SHIELD require further investigation.

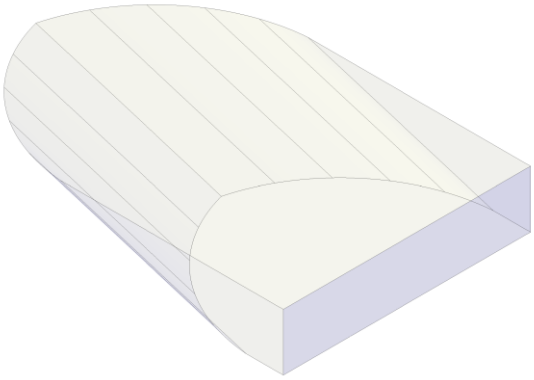

(a)

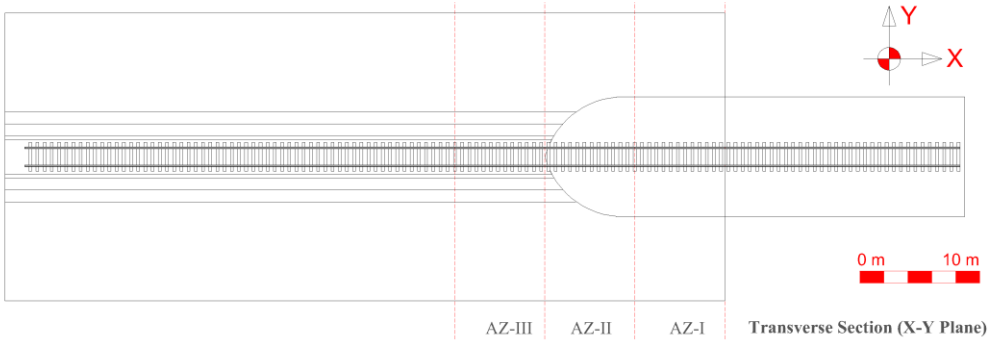

(b)

Figure 3.10. (a) 3D shapes of trapezoidal-shaped SHIELD, (b) transverse cross-section of the model [74].

3.14 Geogrid

The role of geogrids in mitigating natural disasters, such as floods and landslides, should be established with consideration for the specific conditions of each region. Key factors include geotechnical properties, climate conditions, groundwater levels, and surface runoff patterns. In railway applications, geogrids are generally used in two main ways to reinforce track bed

materials [77]. The first involves placing geogrids at the bottom or within the ballast layer, which primarily serves to extend the maintenance cycle by increasing the interval between ballast cleaning and replacement operations. The second method involves installing geogrids beneath the sub-ballast layer, where their main function is to enhance the effective bearing capacity of an underlying soft subgrade. Together, these applications contribute to the long-term stability and performance of rail infrastructure, particularly in challenging environments.

3.15 Concrete confinement walls

Concrete confinement walls (wing walls) are structural elements designed to confine the ballast and subgrade layers, thereby enhancing their stability. These walls can be installed along the transition to prevent ballast migration, increase lateral confinement, and reduce both track deformation and long-term track settlement, see Figure 3.11, [78]. However, this technique leads to higher vertical track stiffness, which can lead to ballast breakage due to higher stress concentrations.

Figure 3.11. Bridge transition zone with concrete confinement wings walls parallel to the track. From [78].

3.16 Universal transition module V-TRAS

The universal transition module V-TRAS has been specifically designed for transition zones between conventional ballasted tracks and ballastless tracks [79]. This module is applicable for embankments, bridges, and various other structural interfaces. Additionally, it is adaptable to narrow, normal, and wide track gauges, as well as light rail systems. V-TRAS consists of a steel ramped structure supported by bearings at the ballastless track end and placed floating on the

ballast bed at the opposite end, as illustrated in Figure 3.12. The structure comprises two longitudinal tapered steel beams, with lengths tailored according to project-specific requirements. Each beam is equipped with supporting plates on top, paired with USPs, arranged according to sleeper spacing. The geometry of these plates and USPs is designed to match the base profile of the concrete sleepers, as depicted in Figure 3.13.

The stiffness and damping properties of the USPs can be customised to meet specific stiffness transition requirements, depending on the unique demands of the transition. The fixation points of the supporting plates on the longitudinal beams are exposed to ballast abrasion, necessitating the use of resilient coatings or elastic pads for protection. The flexural stiffness of the longitudinal beams, combined with the increased vertical stiffness at rail level on the softer side, ensures a gradual stiffness gradient across the transition zone. This design also reduces stress by distributing loads over a larger base area, thereby minimising settlement issues. Compared to other transition solutions, this design offers advantages such as fewer components and the potential for prefabrication, significantly lowering the risk of errors and reducing construction time. The theoretical minimum service life of this system is estimated at 30 years.

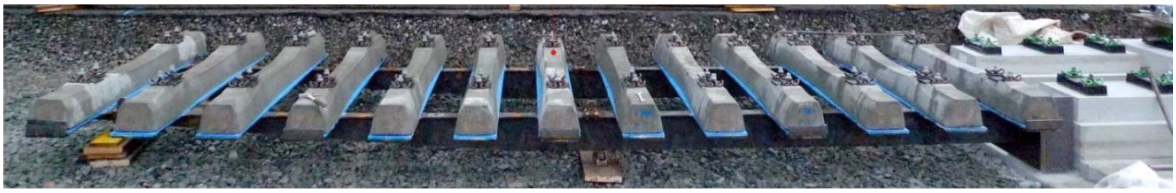

Figure 3.12. The universal transition module V-TRAS pictured as it is provided, supported on the massive end of the ballastless track and floating on the ballast bed [79].

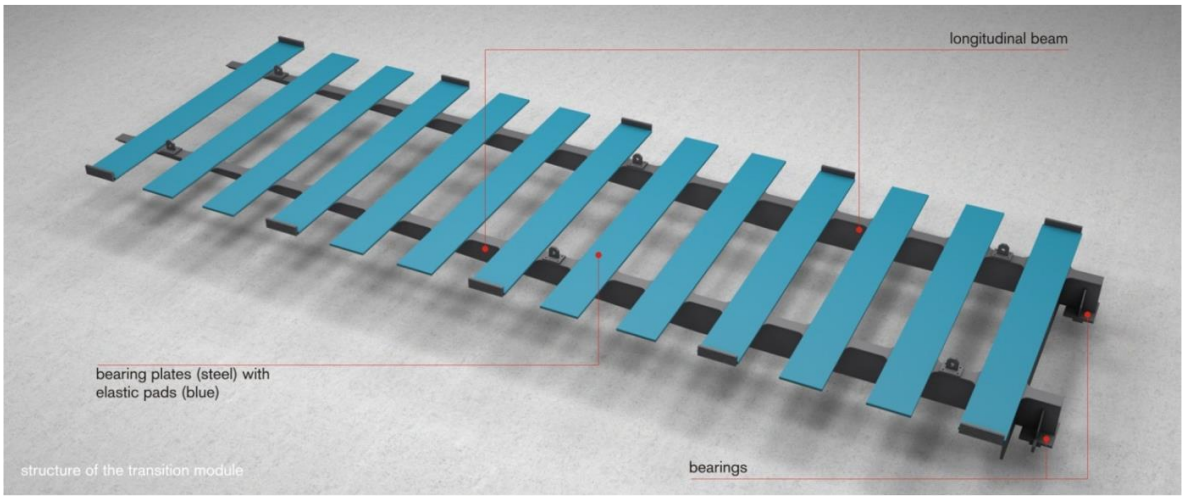

Figure 3.13. The structure of the universal transition module V-TRAS [79].

3.17 Corrective countermeasures

The most common corrective countermeasure is tamping [80]. In this process, sleepers are lifted to the desired level, and the surrounding ballast is packed into the void beneath, either manually or using mechanical equipment. Another approach is stone blowing (either hand-held or track-mounted), [80]. In this method, the sleepers are lifted to the desired level, and a predetermined quantity of stones is blown into the void beneath them using compressed air. The size and number of added stones are determined based on the extent of sleeper displacement and the ballast particle size.

Another corrective countermeasure is the use of the automatic irregularity-correcting sleeper [80]. This type of sleeper consists of a fibre-reinforced polymer body and two automatic subsidence-compensating devices under each rail. The compensating device comprises two nested boxes that allow relative vertical movement. The inner box is connected to the rail via the sleeper, while the outer box rests on the ballast. The inner box is filled with granular material (2 mm in diameter). When differential settlement occurs, the outer box sinks with the ballast, while the inner box remains in position. Adjustable fasteners, comprising two plastic wedges, are inserted between the sleeper and the rail, allowing height adjustment by changing the wedge position. In cases of hanging sleepers, this system can eliminate the void beneath the sleeper and restore full ballast support [80].

4 The Swedish heavy haul line: Traffic load, soil conditions and vehicle model

Malmbanan is a single-track railway line located in the northern part of Sweden. Traffic on the line is dominated by iron ore freight trains with axle loads of 30 – 31 tonnes, operating from the mines in Kiruna and Malmberget to the ports of Narvik (in Norway) and Luleå (see Figure 4.1(a)). The freight cars are equipped with three-piece bogies for support and guidance. The loaded heavy haul trains operate at a speed of 60 km/h, increasing to 70 km/h when empty (tare conditions). In addition to iron ore traffic, the line also accommodates passenger trains running at speeds up to 135 km/h, as well as various other types of freight trains. The annual traffic load is approximately 15 MGT (Mega Gross Tonnes), with around 850 000 axle passages (loaded and unloaded) per year. The track structure comprises 60 kg/m rails, rail fastenings with 10 mm rubber rail pads, and concrete sleepers designed for an axle load of 35 tonnes. The region's extreme climate, featuring winter temperatures reaching as low as −40 °C and relatively warm summers, leads to recurring freeze-thaw cycles and differential settlement, which cause evolving irregularities in the track geometry. The settlement rate along Malmbanan varies significantly, depending on local conditions and subgrade properties.

The present study focuses on monitoring the track response and performance when subjected to loaded iron ore trains. A test site along the line was selected to demonstrate a specific type of slab track. The instrumented section included a transition zone between conventional ballasted track and a 48 m-long demonstrator section of Moulded Modular Multi-Blocks (3MB) slab track. This demonstrator, located in a passing siding at Gransjö, was constructed in September 2022, as part of the Horizon 2020 Shift2Rail EU project In2Track3, and was decommissioned in June 2023.

To reduce the stiffness gradient in the transition area, under sleeper pads were installed along a 15 m section (25 sleepers) of the ballasted track. The 3MB concept is a reinforced, standard precast slab design aimed at facilitating fast and easy maintenance through the use of replaceable precast components. The rail is discretely supported at a rail seat spacing of 0.6 m, and the track is constructed using 4.8 m-long modules. Each module consists of a base slab, formed by two longitudinal reinforced concrete beams connected by two transverse beams, and eight precast moulded concrete blocks, four mounted on each longitudinal beam of the base slab. Elastomeric strips are placed at the interfaces between the base slab and the moulded blocks to provide vibration attenuation and to prevent hammering of the blocks against the base slab (see Figure 4.2).

The subgrade at the site consists almost exclusively of moraine, mixed with big blocks of rock [39], with a maximum depth of 5 m to bedrock. The embankment height varies between 2 and 2.5 m. Due to years of maintenance involving tamping and re–ballasting of the track, the thickness (nominally 30 cm) of the ballast layer has reached 80 cm.

(a) (b)

Figure 4.1. (a) Geographical location of the iron ore line *Malmbanan,* (b) An overview of the transition zone between ballasted track and 3MB slab track at Gransjö, north of Boden.

Figure 4.2. A view of the 3MB slab design consisting of base slabs, top blocks, and an elastomeric layer between the concrete layers.

The iron ore wagon used for heavy haul traffic on Malmbanan includes one car body and two three-piece bogies, each consisting of a bolster, two side frames and two wheelsets. The vehicle model used in **Papers A-B and E-G**, see Figure 4.3, has 14 degrees-of-freedom (DOFs), where two of the DOFs represent the motion (vertical displacement and pitch rotation) of the car body, four DOFs represent the corresponding displacements and rotations of the side frames (two DOFs per bogie), four DOFs the vertical displacement of the four wheelsets, while the four remaining massless DOFs (one per wheelset) are interfacing the rail and are used in the formulation of the constraint equations [81]. In **Paper A**, the 2D vehicle model is validated against a more extensive 3D model in the commercial software GENSYS. In **Paper D**, two bogies from two adjacent wagons are considered. The unsprung mass of each wheelset is denoted M_w. Further, M_b and J_b are the mass and mass moment of inertia for each of the two side frames, while M_c and J_c are the mass and mass moment of inertia for the car body (including

two bolsters). The axle distance within a bogie is Δ_w, while the bogie centre distance is Δ_b. The vehicle model also includes the primary suspension stiffness k_1 and viscous damping c_1, and secondary suspension stiffness k_2 and viscous damping c_2. For traffic on tangent track, it is assumed that the car body and bolster are rigidly connected. Each wheelset is connected to the rail via a Hertzian contact spring.

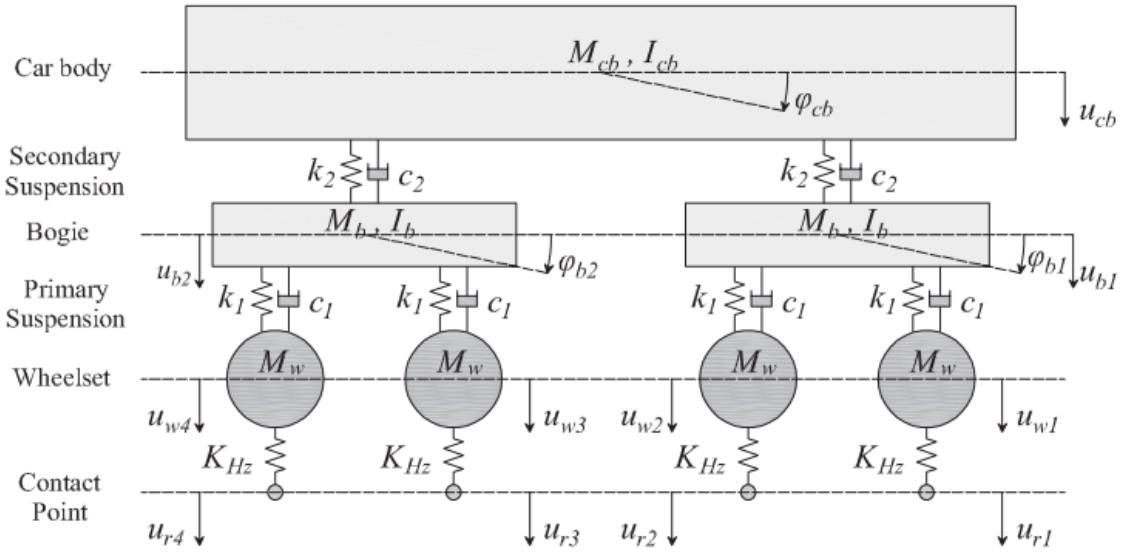

(a)

(b)

Figure 4.3. (a) Vehicle model with ten DOFs consisting of a car body, two bogie frames and four wheelsets [82], (b) iron ore wagon consisting of a car body and two bogies, each consisting of two wheelsets.

5 Track models

5.1 Review of transition zone models

The modelling of a transition zone can be achieved in various ways. In [83], the influences of variations in the foundation stiffness and vehicle speed on the vertical dynamic wheel–rail contact forces were investigated using a 2D FE model, and it was concluded that permanent differential settlement (modelled by updating the longitudinal level of the rail) is the main source of increased wheel–rail contact forces. However, this study considered only a ballasted track model, and the influence of a transition zone was solely modelled by introducing a prescribed variation in rail level and/or foundation stiffness.

Aggestam and Nielsen [8] presented a time-domain 2D model for simulation of vertical dynamic vehicle–track interaction in a transition between ballasted track and slab track using an extended state-space vector approach. Then, by solving a multi-objective optimisation problem using a genetic algorithm, the maximum dynamic loads on the track structure were minimised. It was concluded that the transition zone that had been optimised with respect to both directions of travel resulted in similar dynamic loads as the transition zone which only had been optimised with respect to single-direction traffic. However, this model did not investigate the long-term performance of the transition zone.

Grossoni et al. [15] presented an iterative methodology that couples models of vehicle–track dynamics and long-term track settlement. The dynamic behaviour of the substructure is modelled using an equivalent Lumped Parameter model whose parameters are tuned against a FE model to correctly reproduce the frequency response of the full track. This approach allows for the estimation of evolving track irregularities at locations where track stiffness changes, which in turn leads to increased stresses in the ballast. A settlement model algorithm, accounting for the development of hanging sleepers, is then used in iterative simulations to calculate settlement across individual soil layers.

Wang and Markine [5] coupled a 3D FE model of a transition zone, for simulation of dynamic vehicle–track interaction and stresses in the foundation, with an empirically-based 1D model of resulting settlement per sleeper. The settlement model was applied to consider the linear (long-term) evolution of ballast settlement. It was found that traffic direction involving a gradual increase in track stiffness at rail level, such as from an embankment to a bridge, is a worst-case scenario. Ramos et al [84] studied the short- and long-term behaviour of ballasted and slab tracks subjected to cyclic loading. Settlement of both track forms were compared using laboratory experiments and calibrated numerical models. Using an iterative approach, the two track forms were subjected to three million loading cycles. The calculated settlements were used to develop and calibrate the short-term response of 3D FE models for both track structures. These settlements were then used to modify the 3D model geometry in the subsequent iteration.

Another approach to simulate the complex degradation behaviour of the ballast layer is the use of a discrete element model, see [85]. DEM-based sleeper–ballast models offer a more detailed representation of ballast compared to the vehicle–track–bridge or tunnel models discussed above. However, accurately simulating train loads and dynamic vehicle–track interaction within

a DEM framework remains challenging, which limits its effectiveness in modelling the evolution of hanging sleepers. Because of the extreme computational effort to predict the interaction between individual ballast particles, DEM simulations are typically restricted to short track sections comprising only a few sleepers.

In [86], the simulation results clearly highlighted the significance of particle breakage in the accumulation of permanent ballast deformation under cyclic loading. Most of the particle breakage and the highest rate of permanent strain accumulation were observed to occur during the initial load cycles, with the degradation rate gradually decreasing with increasing number of load cycles. In [87], a bridge–embankment transition zone model was established by combining the DEM with the finite difference method (FDM). In this model, the DEM was used to model sleepers and ballast particles with complex shapes, while the FDM was applied to simulate the abutment, transition section, and embankment. In [34], differential settlement in railway transition zones was simulated using a hybrid DEM–FDM–FEM model without relying on empirical equations, although such simulations involve significantly higher computational costs. This modelling approach is particularly applicable to scenarios requiring a detailed representation of granular ballast behaviour, vehicle–track dynamics, and track-degradation phenomena, albeit over a limited number of load cycles.

In [88], a coupled train–track–bridge (TTB) DEM model of sleepers was proposed, including nonlinear force–displacement behaviour and horizontal interparticle shear, features typically absent in conventional TTB models. This TTB–DEM model was used to examine the influence of hanging sleepers on track dynamics at both sleeper and particle levels. It was concluded that hanging sleepers and underlying ballast provide insufficient support for wheel loads, thereby transferring greater loads to adjacent sleepers. This redistribution of loads exacerbates existing gaps, leads to the formation of additional hanging sleepers, and increases sleeper vibrations, particularly at gap closure. During downward sleeper movement, stronger force chains form, causing particles beneath gaps to gain higher velocities. During upward movement, particles experience stronger interparticle forces and more significant vibrations compared to cases without gaps. Thus, residual forces and kinetic energy within the ballast layer are not fully dissipated due to shorter contact durations in the presence of gaps. A similar model, employing a 3D DEM model framework with a greater number of sleepers, is presented in **Paper G**.

Coelho [89] predicted track settlement on a network scale by considering the effects of stochastic variations in traffic and soil conditions. A semi-analytical, frequency-domain cone model [90], based on the solution of a 1D wave propagation problem, was applied to determine the dynamic stiffness and damping of the soil. A similar approach is used in **Paper A** to calculate the force-displacement relationship for the ballast and subgrade under a sleeper.

5.2 Beam element models

In **Paper A**, a methodology for the simulation of long-term differential track settlement, the development of voided sleepers leading to a redistribution of rail seat loads, and the evolving irregularity in vertical track geometry at a transition between two track forms, is presented. For a prescribed traffic load, the accumulated settlement is predicted using an iterative approach. It is based on a 2D FE time-domain model of vertical dynamic vehicle–track interaction to

calculate the contact forces between sleepers and ballast in the short-term. These are used in an empirical model to determine the long-term settlement of the ballast/subgrade below each sleeper. Gravity loads and state-dependent track conditions are accounted for, including a prescribed variation of non-linear stiffness of the supporting foundation along the track model. Analyses of the influence of higher axle loads and the implementation of USPs on sleeper settlement are demonstrated. The applied model for simulation of dynamic vehicle–track interaction on ballasted track was originally developed by Nielsen and Igeland [81], validated in [91], and extended to slab track in [38].

The non-linear track model in **Paper A** is a FE model with rigid boundaries at both rail ends and at the lower connection point of each spring/damper model representing the ballast and subgrade, see Figure 5.1. The 60E1 rail is modelled by Euler-Bernoulli beam theory with four beam elements per sleeper bay. Each sleeper in the ballasted track section is modelled by a discrete (rigid) element with one vertical DOF and mass. The sleeper distance is taken as uniform, but this is not a constraint of the model. The base slab of the 3MB track is modelled by one continuous beam, below the layer of discrete blocks. Both layers are modelled by Euler-Bernoulli beam theory. Each top block with two rail seats is represented by five beam elements, while the base slab has three beam elements per sleeper bay. It is assumed that the bed modulus [(N/m)/m^2] of the virgin foundation is uniform along and across the track on both sides of the transition. Both linear and nonlinear force displacement relationship for sleeper support spring and damper are investigated. This model was also used for pre-test studies before setting up the measurement campaign at Gransjö.

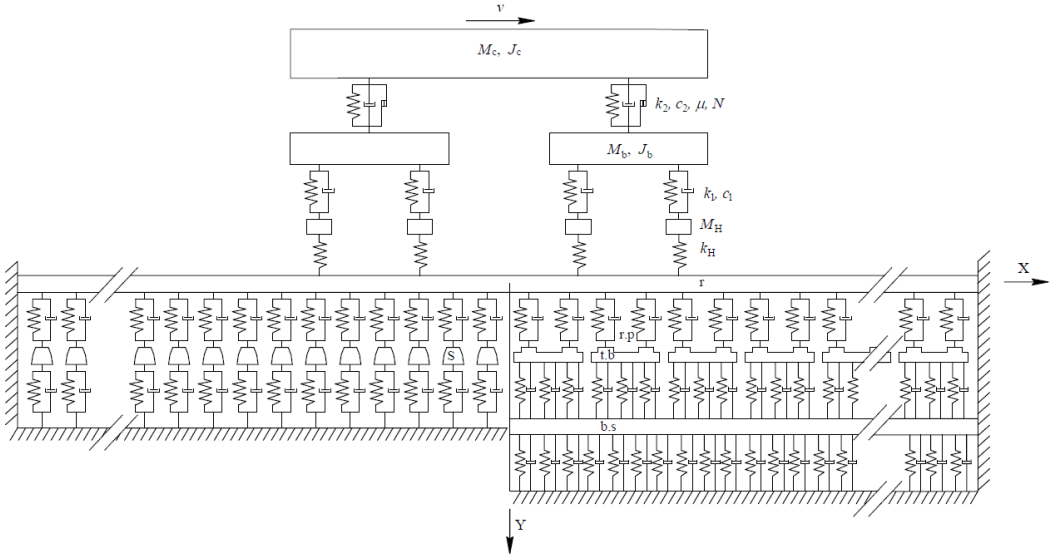

Figure 5.1. Sketch of complete vehicle and transition zone model. The track model contains rail (r), top blocks (t.b) and base slab (b.s) modelled by beam elements. The base slab is supported by a Winkler foundation. The sleepers (s) are rigid masses supported by a spring-damper connection (representing the ballast/subgrade) with non-linear, and potentially random, stiffness properties. From **Paper A**.

In **Papers D and E**, the model from **Paper A** is extended to account for the interaction between sleepers via the ground on the ballasted side. A seven-parameter representation of the ballast and subgrade is employed in the 2D model, see Figure 5.2. These seven parameters include the mass of the ballast (m_b), a state-dependent discrete spring with stiffness (k_b), a viscous damper with damping (c_b) representing the combined properties of the ballast layer and under sleeper pad (USP), and a shear stiffness (k_w) and a shear damping (c_w) to mimic the coupling of the interlocking ballast granules between adjacent ballast masses. Further, the properties of all layers of the subgrade are given by the stiffness (k_{sb}) and the damping (c_{sb}). Based on the measured track receptances at the Gransjö test site, the input parameters for the 2D model have been tuned using the Nelder-Mead optimisation algorithm. A similar iterative approach as used in **Paper A** is applied to simulate long-term differential settlement using the proposed settlement model. Both the settlement model and the track model are calibrated against short- and long-term measured data from **Paper B**. In each iteration step, the bi-linear stiffness characteristics of k_b are updated to account for the potentially evolving voided distance between the sleeper and ballast, where the stiffness becomes zero. Finally, the model is compared with an extensive 3D model developed by Ramos et al. [3]. The vehicle model used in **Paper D** consists of two bogies from two adjacent vehicles, designed to replicate the measured dynamic responses in **Paper B**. It represents a heavy haul wagon with 30-tonne axle loads operating at a speed of 60 km/h.

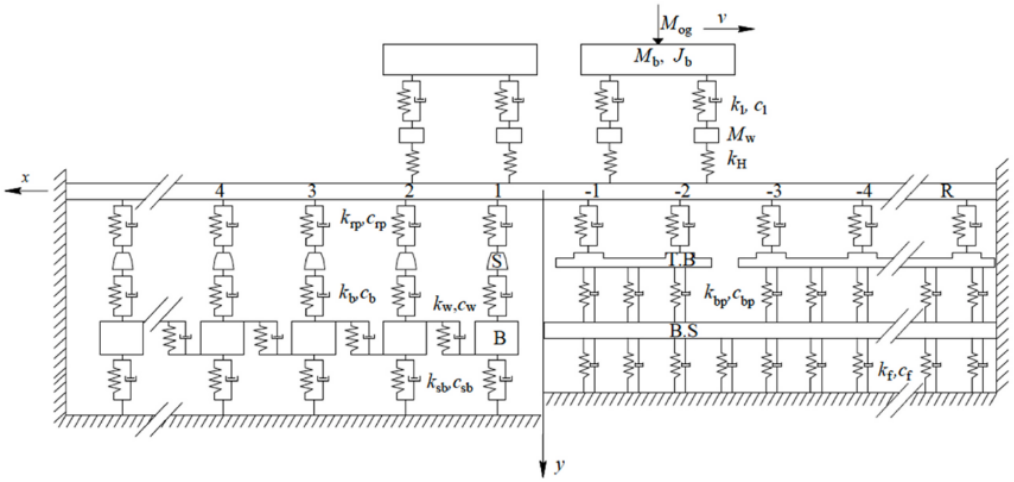

Figure 5.2. Sketch of complete 2D vehicle and transition zone model. The track model contains rail (R), top blocks (T.B) and base slab (B.S) modelled by beam elements. The base slab is supported by a Winkler foundation. The sleepers (S) are rigid masses supported by a seven-parameter model of the substructure using non-linear, and potentially random, properties. The ballast (B) mass is part of the substructure model. From **Papers D** and **E**.

In **Paper E**, the developed model is used to investigate the influence of shorter sleeper spacing and broader sleeper base designs as two strategies to increase the stiffness of the ballasted track and reduce the track stiffness gradient between the two track forms. The goal is to improve the

dynamic vehicle–track interaction in the transition zone and reduce long-term differential settlement at the transition.

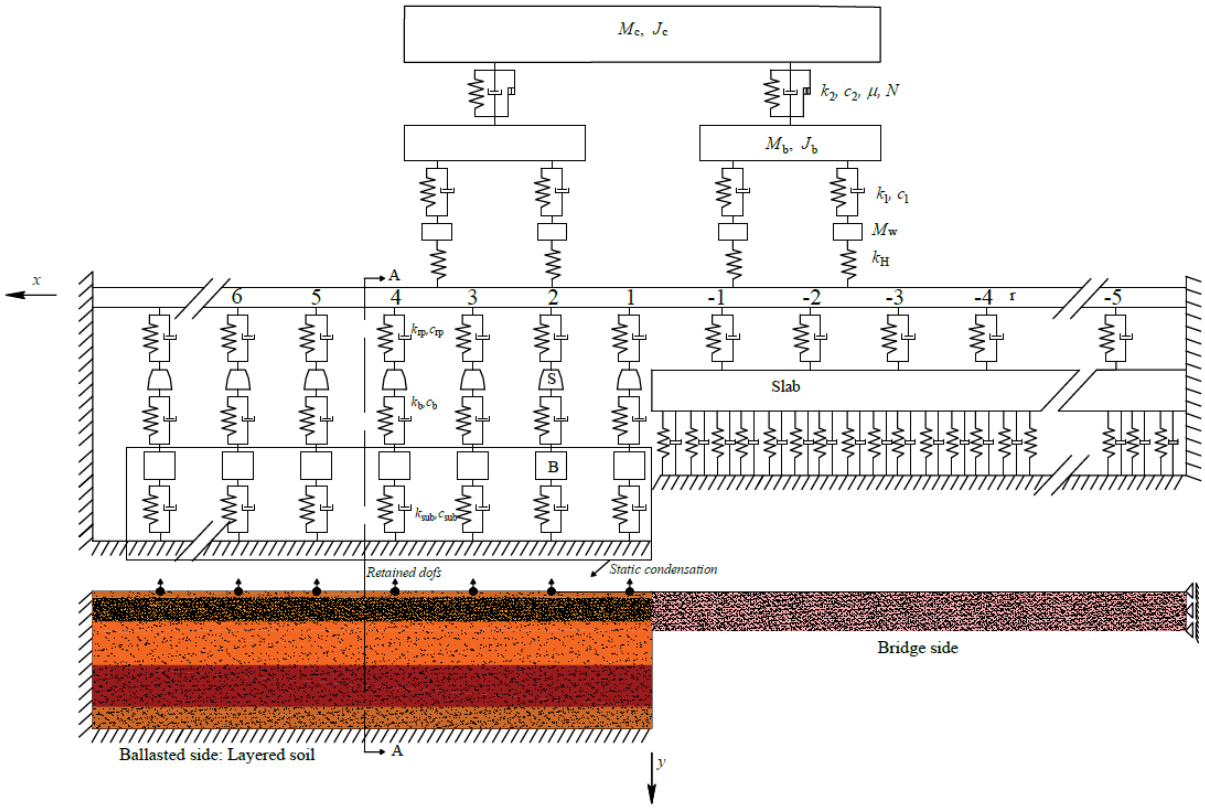

(a)

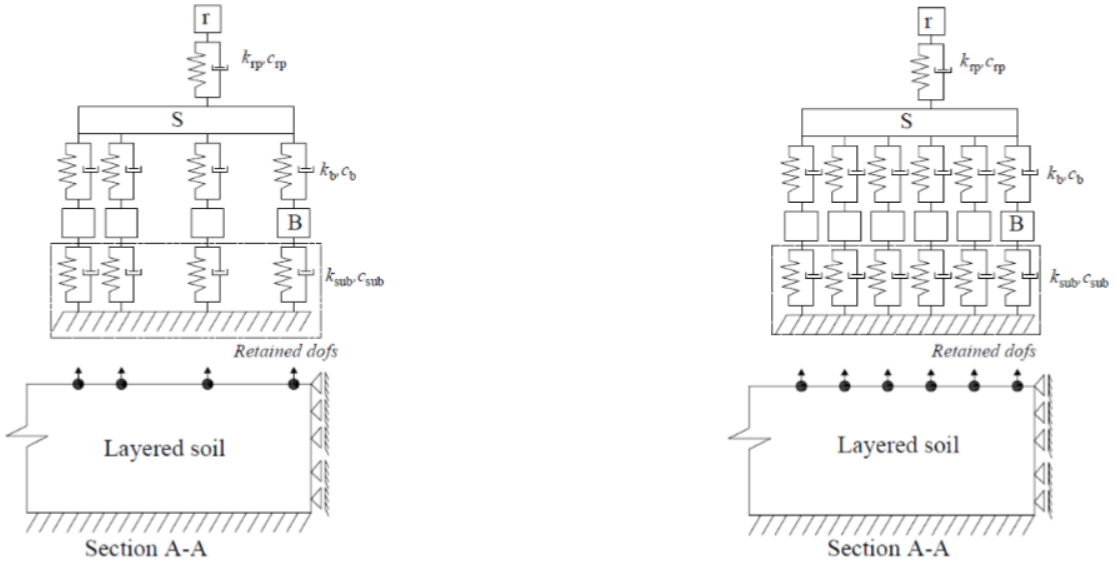

(b) (c)

Figure 5.3: (a) Sketch of complete vehicle and transition zone model, (b) cross-section with sleepers using three beam elements, (c) cross-section with sleepers using five beam elements. Adapted from **Paper F**.

In **Paper F**, a more comprehensive model is introduced, comprising a 2D vehicle model, a 3D non-linear FE model of the track superstructure, and a linear 3D FE model of the layered subgrade. The subgrade model incorporates substructure-based mitigation measures designed to reduce the stiffness gradient at transitions between different track forms. The sleepers are modelled using Euler–Bernoulli beam finite elements, with either three or five elements per half sleeper, see Figure 5.3, while the slab track is represented by a continuous layer of beam elements. To enhance computational efficiency, the subgrade model is simplified using static condensation, resulting in a reduced-order model (ROM). This methodology is applied to evaluate differential settlement occurring in transition zones between ballasted track on embankments and slab track on bridges or in tunnels. Each iteration of the simulation includes a short-term analysis to compute the contact pressure at each sleeper–ballast interface, which is then used as input in an empirical model to predict incremental ballast settlement. A strain analysis is also performed to estimate permanent displacements within the subgrade layers using the Li and Selig approach [92]. The iterative process continues until the prescribed traffic load is reached, enabling the prediction of long-term settlement. The methodology is demonstrated by investigating the effects of implementing a transition wedge on the ballasted (softer) track side, or softer rail pads on the stiffer slab track side. Both directions of vehicle travel are considered in the analysis.

In **Paper G**, a numerical methodology for simulating the mechanisms during the initial phase of differential settlement in a railway transition zone, using an integrated discrete–continuum approach, is presented. The methodology involves the coupling of the DEM, the Finite Difference Method (FDM), and the FEM to model the vertical dynamic interaction between vehicle and transition zone. The 3D DEM model captures the granular behaviour of ballast and sub-ballast, while the FDM represents the rail structure and subgrade, see Figure 5.4. A nonlinear 2D FEM model, combined with a multi-body system (MBS) vehicle model, see Figure 5.5, computes wheel–rail contact forces, which feed into the DEM–FDM simulation to assess evolving permanent displacements. Sleeper support stiffness, used in the FEM, is precomputed from the DEM–FDM coupling through a static load application. The approach captures the void formation beneath sleepers, the redistribution of sleeper–ballast contact forces, and the increasing vertical track irregularities under repeated loading. Applied to a transition zone with a stiffness gradient between a ballasted track and a stiffer track form, the method simulates settlements over 500 axle passages. This hybrid framework offers critical insights into track degradation and the consequences of hanging sleeper vibrations, highlighting the importance of gradual stiffness transitions to mitigate dynamic loading and reduce long-term maintenance needs.

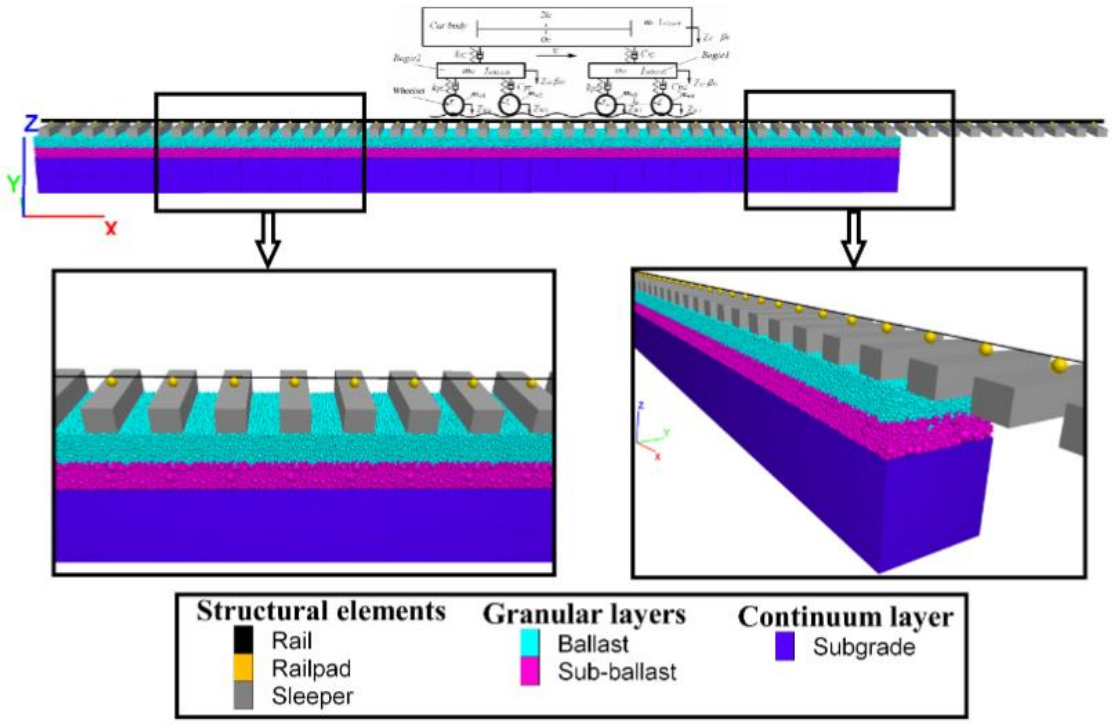

Figure 5.4. Hybrid DEM-FDM-FEM model. From **Paper G**.

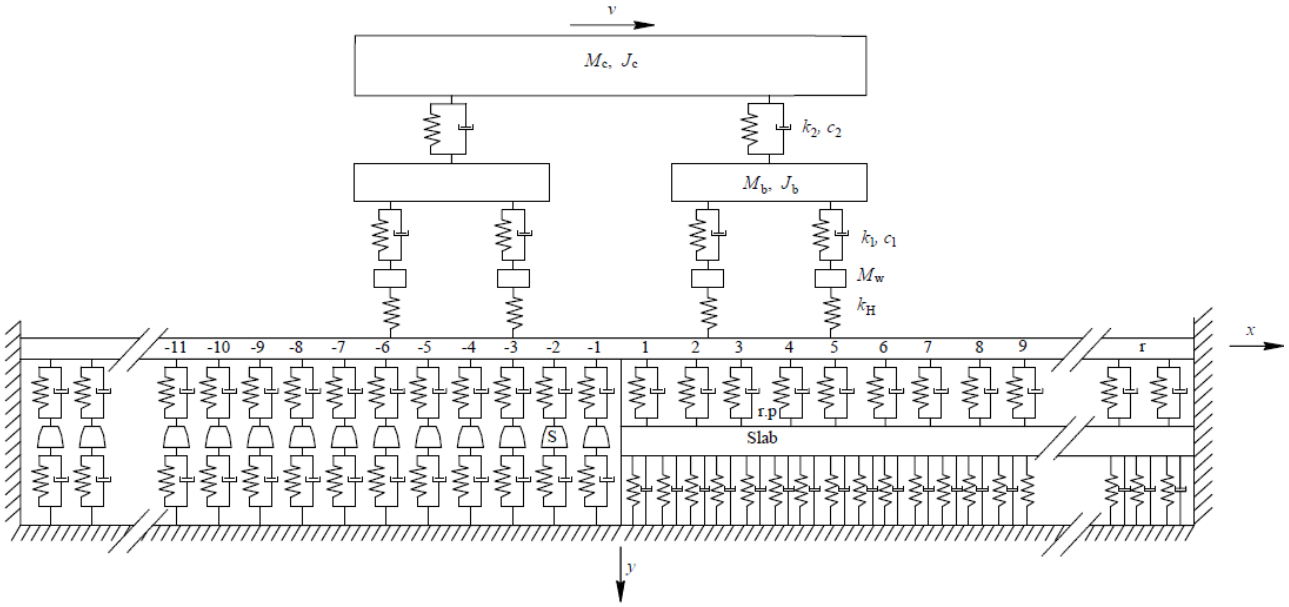

Figure 5.5. Sketch of the complete vehicle and transition zone model (2D MBS-FEM model) including softer (left) and stiffer (right) track forms. The stiffness input data for the sleeper supports are extracted from the DEM model. From **Paper G**.

5.3 Stiffness and damping of subgrade and ballast layers

A semi-analytical, frequency-domain cone model based on 1D wave propagation [90] can be used to estimate the dynamic stiffness and damping of soil. One such approach, proposed by Wolf and Deeks [90], can be used to determine the equivalent stiffness and damping of a layered subgrade. This approach is used in **Paper A** to calculate the stiffness and damping values for the support of each sleeper. Another analytical method by Gazetas [93] can be applied to individual sleepers. In **Paper F**, however, a linear 3D FEM model of the subgrade is developed in ABAQUS to generate an equivalent stiffness matrix. This approach captures also the interactions between multiple foundation points (sleeper nodes) across the transition zone, which is a significant advantage over the previously discussed methods. It is implemented using the *Substructure* command in ABAQUS. However, further work is needed to incorporate also soil dynamics into the model. In **Papers C** and **D**, the subgrade input parameters are calibrated using an optimisation approach to best match the measured receptance data.

5.4 Simulation of vertical dynamic vehicle–track interaction

In this thesis, where the track model is non-linear, the simulation of vertical dynamic vehicle–track interaction is performed by a direct integration in the time domain. A summary of the procedure is given here. For more details, see [11]. An extended (mixed) state–space vector $\boldsymbol{z}(t)$ is introduced as (T denotes the transpose of a vector)

$$\boldsymbol{z}(t) = \{\mathbf{x}^{\mathrm{t,T}} \;\; \dot{\mathbf{x}}^{\mathrm{t,T}} \;\; \mathbf{x}_{\mathrm{a}}^{\mathrm{v,T}} \;\; \mathbf{x}_{\mathrm{b}}^{\mathrm{v,T}} \;\; \dot{\mathbf{x}}_{\mathrm{a}}^{\mathrm{v,T}} \;\; \dot{\mathbf{x}}_{\mathrm{b}}^{\mathrm{v,T}} \;\; \hat{\mathbf{F}}_{\mathrm{a}}^{\mathrm{T}}(t)\} \tag{5.1}$$

It includes the displacements $\mathbf{x}^{\mathrm{t,T}}$ and velocities $\dot{\mathbf{x}}^{\mathrm{t,T}}$ of the transition zone track model. The vertical displacements and velocities of four massless dofs of the vehicle model, that are interfacing the rail are collected in the 4 × 1 vectors $\mathbf{x}_{\mathrm{a}}^{\mathrm{v,T}}$ and $\dot{\mathbf{x}}_{\mathrm{a}}^{\mathrm{v,T}}$, respectively, while $\mathbf{x}_{\mathrm{b}}^{\mathrm{v,T}}$ and $\dot{\mathbf{x}}_{\mathrm{b}}^{\mathrm{v,T}}$ are two 10 × 1 (in **Paper D**, 8 × 1) vectors containing the vertical displacements and velocities of the non-interfacial vehicle dofs, representing the motion of a full vehicle (two adjacent bogies in two adjacent iron ore wagons). Further, it contains the impulses $\hat{\mathbf{F}}_{\mathrm{a}}^{\mathrm{T}}(t) = \int \mathbf{F}_{\mathrm{w/r}}(t)\ \mathrm{d}t$ of the wheel–rail contact forces. All equations of motion for vehicle and track, and the algebraic constraint equations coupling the vehicle and track, are assembled in one first-order matrix form as

$$\mathbf{A}(\boldsymbol{z},t)\dot{\boldsymbol{z}} + \mathbf{B}(\boldsymbol{z},t)\boldsymbol{z} = \mathbf{F}(\boldsymbol{z},t) \tag{5.2}$$

with

$$\mathbf{A}(\boldsymbol{z},t)=\begin{bmatrix}\mathbf{0} & \mathbf{M}^{\mathrm{t}} & \mathbf{0} & \mathbf{0} & \mathbf{0} & \mathbf{0} & -\mathbf{N}^{\mathrm{T}}\\ \mathbf{I} & \mathbf{0} & \mathbf{0} & \mathbf{0} & \mathbf{0} & \mathbf{0} & \mathbf{0}\\ \mathbf{0} & \mathbf{I} & \mathbf{0} & \mathbf{0} & \mathbf{0} & \mathbf{0} & \mathbf{I}\\ \mathbf{0} & \mathbf{0} & \mathbf{0} & \mathbf{0} & \mathbf{0} & \mathbf{M}^{\mathrm{v}}_{\mathrm{bb}} & \mathbf{0}\\ \mathbf{0} & \mathbf{0} & \mathbf{0} & \mathbf{I} & \mathbf{0} & \mathbf{0} & \mathbf{0}\\ \mathbf{T} & \mathbf{0} & \mathbf{0} & \mathbf{0} & -\mathbf{I} & \mathbf{0} & \mathbf{0}\\ \mathbf{R} & \mathbf{0} & -\mathbf{I} & \mathbf{0} & \mathbf{0} & \mathbf{0} & \mathbf{0}\end{bmatrix} \tag{5.3}$$

$$\mathbf{B}(\boldsymbol{z},t)=\begin{bmatrix}\mathbf{K}^{\mathrm{t}} & \mathbf{C}^{\mathrm{t}} & \mathbf{0} & \mathbf{0} & \mathbf{0} & \mathbf{0} & \mathbf{0}\\ \mathbf{0} & -\mathbf{I} & \mathbf{0} & \mathbf{0} & \mathbf{0} & \mathbf{0} & \mathbf{0}\\ \mathbf{0} & \mathbf{0} & \mathbf{K}^{\mathrm{v}}_{\mathrm{aa}} & \mathbf{K}^{\mathrm{v}}_{\mathrm{ab}} & \mathbf{0} & \mathbf{0} & \mathbf{I}\\ \mathbf{0} & \mathbf{0} & \mathbf{K}^{\mathrm{v}}_{\mathrm{ba}} & \mathbf{K}^{\mathrm{v}}_{\mathrm{bb}} & \mathbf{0} & \mathbf{C}^{\mathrm{v}}_{\mathrm{bb}} & \mathbf{0}\\ \mathbf{0} & \mathbf{0} & \mathbf{0} & \mathbf{0} & \mathbf{0} & -\mathbf{I} & \mathbf{0}\\ \mathbf{U} & \mathbf{0} & \mathbf{0} & \mathbf{0} & \mathbf{0} & \mathbf{0} & \mathbf{0}\\ \mathbf{S} & \mathbf{0} & \mathbf{0} & \mathbf{0} & \mathbf{0} & \mathbf{0} & \mathbf{0}\end{bmatrix} \tag{5.4}$$

Here $\mathbf{M}^{\mathrm{t}}$, $\mathbf{K}^{\mathrm{t}}$, and $\mathbf{C}^{\mathrm{t}}$ are the mass matrix, stiffness matrix and viscous damping matrix of the track model, whereas $\mathbf{K}^{\mathrm{v}}$, $\mathbf{M}^{\mathrm{v}}$ and $\mathbf{C}^{\mathrm{v}}$ are the corresponding matrices for the vehicle model. Each wheel–rail contact force is distributed as consistent forces and moments on the adjacent rail nodes using Hermitian interpolation polynomials. By assuming a prescribed vehicle speed v(t) and considering the Coriolis and centripetal accelerations that occur because the vehicle model is moving along the track model, the constraints on the interfacial velocities and accelerations for the massless dofs of the vehicle model are expressed in **R**, **S**, **T**, and **U** cf.[11] . The mixed force vector **F** is written as

$$\mathbf{F}(\boldsymbol{z},t)=\{\mathbf{F}^{\mathrm{t,T}}_{\mathrm{s/b}}(t)+\mathbf{F}^{\mathrm{t,T}}_{\mathrm{g}}\ \ \mathbf{0}^{\mathrm{T}}\ \ \mathbf{0}^{\mathrm{T}}\ \ \mathbf{F}^{\mathrm{v,T}}_{\mathrm{b}}(t)\ \ \mathbf{0}^{\mathrm{T}}\ \ \dot{\mathbf{x}}^{\mathrm{irr}}\ \ \ddot{\mathbf{x}}^{\mathrm{irr}}\}^{\mathrm{T}} \tag{5.5}$$

where the vector $\mathbf{F}^{\mathrm{t,T}}_{\mathrm{s/b}}$ contains the state-dependent contribution to the sleeper–ballast force acting on each sleeper in the ballasted track section (note that any stiffness of the bi-linear spring k_{b} up to the breakpoint representing the voided distance between sleeper and ballast is considered in $\mathbf{K}^{\mathrm{t}}$), while the constant vector $\mathbf{F}^{\mathrm{t,T}}_{\mathrm{g}}$, includes the gravity load on the track superstructure. Further, prescribed external loads (vehicle gravity loads) are assembled in $\mathbf{F}^{\mathrm{v,T}}_{\mathrm{b}}$, while $\mathbf{x}^{\mathrm{irr}}$ contains the prescribed wheel/rail surface irregularities.

The initial value problem for the solution of the transient vibration problem is written as

$$\dot{\boldsymbol{z}}=\mathbf{A}^{-1}(\mathbf{F}-\mathbf{B}\boldsymbol{z}),\ \boldsymbol{z}(t=0)=\boldsymbol{z}_0 \tag{5.6}$$

where $\boldsymbol{z}_0$ includes the initial state due to the weight (gravity load) of the track. In the present study, the solution is obtained using MATLAB's moderately stiff differential equation solver ode23s with an adaptive time step.

6 Settlement models

6.1 Review

Railway tracks are subjected to dynamic traffic loading from trains operating at varying speeds and axle loads. The cyclic loading leads to a time-variant vertical deformation of the track. A small part of this vertical deformation is permanent, meaning that after a train has passed, the track will not fully return to the same position as before the train arrived. In addition to the stresses induced by quasi-static and dynamic wheel loads, geostatic stresses contribute to the long-term settlement. Over time, these small permanent deformations accumulate over a large number of loading cycles, potentially leading to substantial differential settlement affecting track geometry. For example, granular aggregates such as ballast densify under cyclic loading, reducing their void ratio as particles rearrange and settle into a more compact configuration [94].

According to Refs. [33,95], higher dynamic loads in a transition zone, induced by a gradient in vertical track stiffness and/or an initial misalignment in rail level, are key contributors to track deterioration through differential ballast settlement. As a consequence of differential settlement, track geometry irregularities evolve, which in turn alter the distribution of loads [96]. The rate of differential settlement depends on several factors, such as the type and amount of traffic (e.g., axle load, train speed, dynamic vehicle–track interaction, accumulated traffic load), the design of the superstructure (rail and sleeper type, sleeper spacing, stiffness of rail pads and any additional resilient layers like USPs that all influence how loads are distributed onto the ballast and subgrade), and properties of the layered substructure (depth, density, stiffness or resilient modulus, ballast specification in terms of particle size distribution and mineralogy, ballast contamination, drainage and pore water pressure conditions).

Extensive reviews of settlement models have been presented by Dahlberg [31], Abadi et al. [97], Rempleos et al. [98], and Grossoni et al. [99]. Dahlberg [31] concluded that the magnitude of track settlement depends on the quality and behaviour of the ballast, sub-ballast and subgrade, and that there are two basic phases of settlement. The first phase corresponds to a higher settlement rate soon after construction of the line or after maintenance tamping, while the second phase shows a slower settlement rate that generally decreases with the accumulation of traffic load. The initial phase of ballast settlement can be attributed to the compaction of the ballast. After the ballast achieves a higher density, the second phase of ballast settlement begins to dominate. This second phase of settlement may be characterised by particle damage/fracture and further particle rearrangement. It is controlled by several factors, including deviatoric stresses, vibrations, degradation, and subgrade stiffness [31,97,100–102].

Constitutive models accounting for the complex elastoplastic behaviour of geomaterials have been implemented in 2D and 3D FE models, but are generally associated with a high computational cost, see e.g. [3,32,44]. The most widely used model to describe the non-linear stress-dependent stiffness of unbound granular materials (such as ballast) is the $K - \Theta$ model, or power law model, see [103,104]. Compared with using a constitutive model, results from

empirical models have been reported to be similar in accuracy, yet they depend on a much smaller number of input parameters [3].

Empirical equations, which are mechanistic or physical models based on prior physical information, have been used to quantify and characterise track settlement. These equations have two primary forms: logarithmic [95] and exponential [97]. The settlement is calculated as a function of the number of load cycles and the settlement after the first load cycle. In tests with up to millions of load cycles, measured track settlement versus number of load cycles has generally shown the phases previously described by Sato [105] and Dahlberg [31]. To improve agreement with experimental data, more complex empirical equations have been developed. The models proposed by Grossoni et al. [99] and Ognibene et al. [106], which use vertical stress in the ballast and sleeper–ballast contact force as driving parameters, respectively, are considered semi-empirical approaches.

Most empirical equations have been developed for the ballast (granular) layers. Similarly, empirical parameters for predicting subgrade settlement have been derived from laboratory tests conducted under various soil conditions, aimed at investigating plastic deformation under repeated loading [17,92,107,108]. The total accumulated settlement over the long term is calculated by summing the accumulated settlement increments from both the ballast and subgrade layers. Extensive 3D numerical models can be used to calculate settlement over a defined number of wheel passages without relying on empirical models. While this approach is computationally intensive and generally not recommended for long-term simulations, it offers valuable insights into the initial stages of long-term differential settlement. A similar approach is used in **Paper G**.

Sato [105] proposed an empirical equation in which track settlement is expressed as a function of the number of load cycles and the sleeper–ballast contact pressure, or sleeper–ballast contact force. Here, the settlement is proportional to the square of the difference between the sleeper–ballast contact pressure and a threshold pressure value. Dahlberg [31] later extended this model by generalising the exponent from 2 to n. By calibrating the model against laboratory test data, a better fit was obtained for n values in the range of 4 – 5, within the investigated range of contact pressures. It was suggested that different degradation or failure mechanisms may dominate across different loading ranges.

To simulate the settlement increment induced by each passing vehicle, or even each passing wheel, would entail a high computational cost. A common technique to address this problem is to use an integrated approach where a numerical model of the dynamic vehicle–track interaction in the short term is combined with an empirical model of the long-term settlement. For example, Sayeed and Shahin [109] considered the effect of a moving dynamic vehicle load and applied a 3D FE model to compute the deviatoric stresses in the foundation that were then used as input in an empirical settlement model. A cyclic domain model integrated with an iterative approach to compute differential track settlement, accounting for longitudinal variations in load and track properties, was developed by Li et al. [44]. Similar techniques have been used to predict settlement in transition zones, see [3,41].

In recent years, machine learning techniques have gained popularity among researchers as tools for modelling geometric degradation of railway tracks. For track geometry prediction, a broad spectrum of data-driven predictive models has been investigated in studies documented in the

literature [110,111], including linear and exponential functions, stochastic models, and Markov chains. These models can be used to predict the degradation of a track section over time. Given the ability of machine learning techniques to discover patterns in noisy and complex datasets, they are strong candidates for capturing spatial variations in geometry degradation parameters [98,110,111].

Although numerous studies have examined the shape, wavelength, and amplitude of train-induced settlements based on vehicle response data analysed using machine learning [112] and deep learning [113,114], these approaches depend on a stable relationship between vehicle response and track excitation, assuming ideal conditions such as continuous wheel–rail contact, which may not always be the case in practice. Isolating settlement components from track irregularity data is challenging without a sufficiently large dataset of settlement signals [115]. A review of different machine learning approaches used to predict settlement in transition zones, along with their application to the case study presented in **Paper B**, is presented in [116].

6.2 Settlement models applied in the thesis

6.2.1 Visco-plastic threshold model for ballast layers

The settlement model (threshold function) used in **Papers A-D** is conceptually similar to the one suggested by Sato [105], and later extended by Dahlberg [31], in the sense that there is no accumulation of permanent ballast/subgrade deformation if the maximum sleeper–ballast contact force generated by a passing wheel is below a particular threshold value. In these papers, it is assumed that the model accounts for the overall permanent deformation across all layers of the substructure, including the subgrade.

In **Papers A-D**, after solving the short-term dynamic vehicle–track interaction, the time history of each sleeper–ballast contact force is calculated in a post-processing step using the FE model of the track. For each vehicle model passage in iteration step j (j = 1, 2, … n_s), the incremental settlement $\delta_{i,j}$ [m] at sleeper i (i = 1, 2, … N_{bays}-1) is formulated as a function of the maxima of the sleeper–ballast contact force $F_{s/b,i}$

$$\delta_{i,j} = \sum_{n=1}^{N_w} \left\{ \sum_{k=1}^{N_k} \alpha_k \left[\frac{\langle \max\,(F_{s/b,i})_n - F_{th,i} \rangle}{F_0} \right]^{\beta_k} \right\} \tag{6.1}$$

where N_w is the number of wheels in the vehicle model. Within a given iteration step, it is assumed that the set of max ($F_{s/b,i}$) remains the same for all vehicle passes such that a linear extrapolation of the settlement increment to represent up to 10^5 load cycles can be carried out, see the further discussion below. The order N_k of the polynomial formulation and the corresponding parameters α_k and β_k are empirical, while F_0 = 1 kN is a reference contact force such that the term within the square brackets becomes non-dimensional. In this settlement model, there is no accumulation of permanent ballast deformation if the maximum sleeper–

ballast contact force generated by a passing wheel is below a certain threshold value $F_{th,i}$, as reflected in Equation (6.1) by the Macaulay brackets.

The accumulated settlement at sleeper i after n_s iteration steps (corresponding to N_s wheel passings) is calculated by summing the incremental settlements calculated for each preceding step j as

$$\Delta_i(n_s) = \sum_{j=1}^{n_s} \delta_{i,j} \tag{6.2}$$

In the next iteration step, the accumulated settlements are applied in the bi-linear ballast stiffness descriptions of the updated track model. For each sleeper i, it is assumed that the current threshold value $F_{\mathrm{th},i}$ is dependent on the accumulated settlement Δ_i as

$$F_{th,i}(\Delta_i) = F_{th,\infty} - \left(F_{th,\infty} - F_{th,0}\right)e^{-\gamma\Delta_i} \tag{6.3}$$

where $F_{\mathrm{th},0}$ is the virgin threshold value before any traffic loading has been applied, $F_{\mathrm{th},\infty}$ is the long-term threshold value corresponding to a completely stabilised (consolidated) track, while γ is a parameter that determines the rate of hardening. As inspired by a visco-plastic material mechanics formulation, the threshold value is dependent on the accumulated settlement. This leads to a non-linear hardening (increase) of the threshold value with increasing settlement and consequently to a decreasing settlement rate with increasing accumulated traffic load. The parameters of the threshold value are track site-specific. These parameters (as well as α_k and β_k) are calibrated against field measurements in **Papers B and D**.

In each iteration step, up to 10^5 load cycles (corresponding to 3 MGT of traffic with loaded iron ore trains) are considered. However, an adaptive step length is applied such that the maximum allowed settlement increment $\delta^{\max}$ per iteration step is limited. If the increment exceeds $\delta^{\max}$, a linear interpolation is applied. A convergence study on the influence of the settlement increment per iteration step on the accumulated settlement was presented in [43], and it was concluded that $\delta^{\max} = 0.2$ mm provides a reasonable compromise between accuracy and computational cost.

To summarise, the simulation model applied in **Papers A and C-D** is based on an iterative approach where a time-domain model of vertical dynamic vehicle–track interaction in the short term (accounting for voided sleepers and state-dependent properties of the ballast and subgrade at each sleeper–ballast interface) is integrated with an empirical model of accumulated ballast and subgrade settlement in the long term, see also [43]. The simulation procedure is illustrated in Figure 6.1. In each iteration step, a time-domain simulation of short-term vehicle–track dynamics is performed, using the pre-calculated static track displacement due to gravity load as initial conditions. The calculated load maxima at the interface between each sleeper and ballast in the ballasted track section, generated by the combination of gravity load and each of the passing wheels of the vehicle model, are extracted and used as input to an empirical settlement model. In each iteration step, the track model is updated to account for the current states of the support conditions, and it is assumed that the same set of load maxima is generated by all passing vehicles. By taking several iteration steps, the accumulated differential settlement in

the long term, the potential development of voided sleepers, and the resulting redistribution of foundation loads between adjacent sleepers are calculated.

The settlement model has also been revised to use the maximum values from the time history of sleeper–ballast contact pressures in the post-processing step instead of the maximum sleeper–ballast contact forces. This modified approach is applied in **Paper D** to compare long-term differential settlement in a transition zone with different designs. In that study, only settlement due to the ballast is considered. In **Paper F**, the maximum pressure beneath each sleeper element (in a flexible sleeper model) is used as input to compute long-term differential settlement within a 3D model.

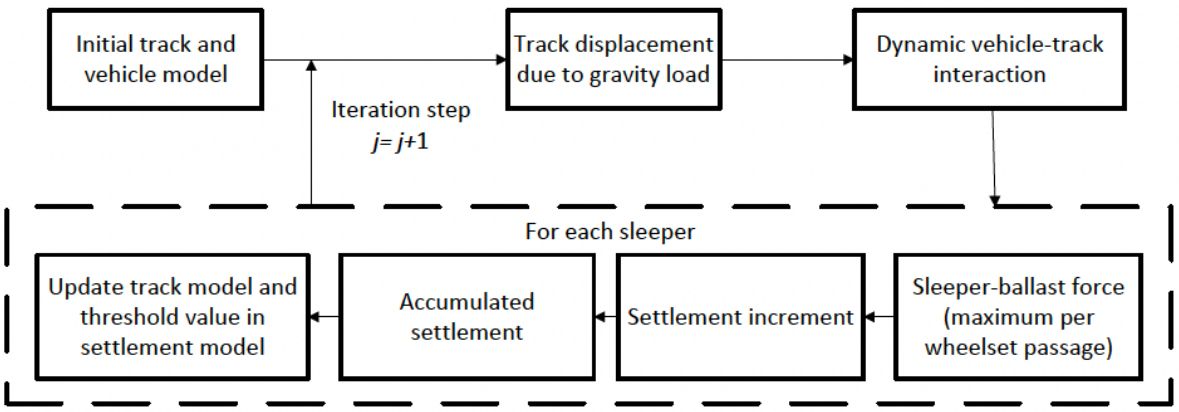

Figure 6.1. Iterative procedure to predict differential settlement in a transition zone. From **Papers A and C-D**.

6.2.2 Settlement in subgrade layers

Numerous models have been developed to predict the permanent deformation (or strain) of railway ballast or subgrade materials. Among these, the majority are formulated as power-exponential equations involving the number of load cycles and dynamic stress, such as the power-exponential model proposed by Li and Selig [92]. For each sleeper number i, the formula proposed by Li and Selig [92], and later modified by Charoenwong et al. [107], can be used to predict the increment in permanent deformation at different depths of the subgrade

$$\Delta\varepsilon_{i,j}^{\mathrm{p}}(y) = \frac{a}{100}\left(\frac{\sigma_d(y)}{\sigma_s(y)}\right)^m \left(N_j^b - N_{j-1}^b\right) \tag{6.4}$$

where $\Delta\varepsilon_{i,j}^{\mathrm{p}}(y)$ is the subgrade plastic strain increment at depth y, $\sigma_d(y)$ denotes the corresponding deviatoric stress due to traffic load (N/m²), N_j^b is the total number of wheel passages including iteration j, while N_{j-1}^b is the total number of wheel passages including iteration $j-1$. In this study, the deviatoric stress is calculated using the Flamant solution [117], which provides analytical expressions for stresses induced by a surface unit load (here the

sleeper–ballast contact force at sleeper *i*) on a semi-infinite, layered elastic medium, directly beneath the vertical point load at a given depth *y*. There are different approaches to calculate the deviatoric stress in the different layers, such as using empirical formulae $\sigma_d = \sigma_{d,0} e^{-0.279h}$, with $\sigma_{d,0}$ denoting the stresses of the layered soil surface and h the depth of each layer from the surface [113]. Alternatively, these stresses can be extracted from extensive 3D FE models of layered soils [118] or derived from traditional analytical solutions, such as those by Timoshenko and Goodier [119]. The term $\sigma_s(y)$ represents the compressive strength of the soil layer at depth *y* (N/m²), while *a*, *b*, and *m* are parameters that depend on the type of subgrade soil.

The subgrade is discretised with H_k elements in the depth direction, with corresponding element heights h_k. In step *j*, the increment $\delta_{i,j}^{\mathrm{sub}}$ in total permanent deformation of the layered subgrade is calculated by using the layer wise summation method

$$\delta_{i,j}^{\mathrm{sub}} = \sum_{k=1}^{H_k} \left(\Delta\varepsilon_{i,j}^{\mathrm{p}}(k)\right) h_k \tag{6.5}$$

The accumulated settlement of the layered subgrade for each sleeper *i* after n_s iterations (corresponding to N_s wheel passages) is

$$\Delta_{i,j}^{\mathrm{sub}} = \sum_{j=1}^{n_s} \delta_{i,j}^{\mathrm{sub}} \tag{6.7}$$

The total accumulated settlement at each sleeper node is determined by summing the settlements of the ballast and subgrade layers. In **Paper F**, the settlement (permanent displacement) of the ballast is predicted using the viscoplastic threshold model, while the settlement in the subgrade layers is estimated based on the approach proposed by Li and Selig [92].

7 Condition monitoring in transition zones

7.1 Background and introduction

Several field investigations have been conducted to assess railway performance, with particular emphasis on transition zones and the monitoring of differential settlement. The monitoring techniques employed can be broadly categorised into trackside monitoring, onboard monitoring, and inspection methods. Trackside monitoring involves the deployment of instrumentation either within or adjacent to the track to observe the track structure, the vehicles passing over it, or the interactions between the two [120]. For the track, this includes observing the status of various track layers, their geometry, and how they evolve over time [121]. On the other hand, onboard track monitoring and inspection are generally carried out using in-service vehicles, as their regular passing over longer sections of track allows for efficient monitoring of track status. Onboard component monitoring is carried out by instrumentation on vehicles, evaluating their condition over time. Dedicated vehicles are equipped with advanced equipment that enables in-depth inspections, which are vital for railway safety. However, these vehicles require special scheduling and trained personnel, limiting their usage [122]. Measurement units on these vehicles use technologies such as laser imaging, image processing, Ground Penetration Radar (GPR), ultrasonic sensors, vibration sensors, high-precision accelerometers, and electromagnetic sensors.

Several in situ investigations utilising trackside monitoring have been conducted to assess the dynamic behaviour of railway tracks using instruments, such as accelerometers, strain gauges, and displacement transducers [7,123]. Coelho [26] presented the results from an extensive monitoring campaign of transition zones (embankment-culvert) in the Netherlands. Vertical displacement at various depths of ballast and subgrade, axle load, and average track stiffness were measured using geophones, uniaxial accelerometers (placed within the ballast), triaxial accelerometers (positioned within the soil below the track), strain gauges, and a high-speed camera. It was concluded that voided sleepers in the transition zone, resulting from long-term differential track settlement, were the primary sources of large track displacements that led to increased impact loading and accelerated track degradation. Fortunato et al. [44] investigated a wedge-shaped approach slab in a transition zone and concluded that a gradual transition of vertical stiffness can be achieved with this approach.

Structural health monitoring of rail tracks and transition zones can be carried out using conventional track geometry cars and other advanced techniques, such as digital image correlation (DIC) and satellite synthetic aperture radar (InSAR) systems [13]. In Wang et al. [124], dynamic rail displacements at multiple points in transition zones were measured without track possession, providing the dynamic displacement profile of the transition zone. It was concluded that permanent rail displacements near the bridge were larger than elsewhere.

In [125], a track deflection and stiffness survey were carried out using micro-electro-mechanical-systems (MEMS) accelerometers. About 80 of these devices were placed on successive sleeper ends, primarily on the field side of the double track, and then moved along the site during consecutive night-time possessions. This was done in two batches of 200

sleepers, with an overlap of 50 sleepers between the batches. Measurements were repeated approximately three months apart. The devices were programmed to record continuously at a frequency of 400 Hz. The acceleration signals were filtered and integrated twice to reconstruct displacements, using 4^{th}-order high- and low-pass Butterworth filters with cut-on and cut-off frequencies of 2 and 40 Hz, respectively [37]. Furthermore, a webcam mounted on a telescope was positioned 6 m from the track to minimise the influence of ground vibrations. It captured images of a target mounted on the sleeper, enabling the measurement of peak-to-peak displacement. However, a key limitation of this method was that the video recording system could monitor the displacement of only one or two sleepers at a time. Additionally, this measurement could be inaccurate depending on train speed. The frequencies dominating the dynamic track response during the passage of trains vary depending on the bogie spacing and train speed. Thus, when a dominating frequency exceeds a specific value, the result can be underestimated due to the camera's low acquisition rate. For high-speed train operation, a higher frame rate is required, such as 150 Hz.

Optical fibre sensors offer significant advantages over conventional and other smart sensors due to their high sensitivity, small size, and potential for short- and long-distance measurement. For example, Wheeler et al. [49,126] measured rail strains using Rayleigh backscattered, distributed optical fibre sensors. Their field test instrumentation included a 7.5 m long section of rail with nylon-coated single-mode fibres installed on the rail web at 20 mm and 155 mm from the bottom of the rail. The measured rail strains were used to determine shear forces, which, together with the known static wheel loads, were employed as part of the calibration to determine the rail seat loads for 14 consecutive sleepers as the train traversed the instrumented track. These data were then combined with measurements of dynamic rail displacement captured through high-speed imaging using digital image correlation (DIC) to process the rail seat load–deflection relationships for each sleeper.

On-board monitoring techniques have been investigated in research and used in infrastructure management [127]. This leads to better maintenance planning and reduces the delay between decision-making and the execution of maintenance actions. For example, in Finland, ballast degradation due to traffic and freeze-thaw cycles, leading to further particle breakage, settlement, or heaving, has been investigated using track geometry recording cars [128]. In Sweden, vertical track geometry degradation between 1999 and 2016 has been studied using regular monitoring by track geometry recording cars [129,130]. Furthermore, in Switzerland, an onboard monitoring policy is considered in infrastructure maintenance planning [131], and similarly in Australia [132].

In **Paper B**, the performance of a selected transition zone on the Swedish Iron Ore Line was investigated through a comprehensive monitoring program that included both onboard and trackside monitoring. The program consisted of long-term and short-term condition monitoring. The long-term measurements focused on the static track behaviour to evaluate the influence of accumulated loading on the degradation of the transition zone. In contrast, the short-term measurements targeted the dynamic response of the track during the passage of various types of trains.

7.2 Fibre Bragg gratings

Fibre Bragg gratings (FBG) are periodic patterns of varying refractive index along the length of the core of an optical fibre, creating a fixed index modulation. At each change of periodic refraction index, a small amount of light is reflected. All the reflected light signals combine coherently to one significant reflection at a particular wavelength when the grating period is approximately half the wavelength of the light input. This phenomenon is referred to as the Bragg condition, and the wavelength at which this reflection occurs is known as the Bragg wavelength. Light signals at wavelengths other than the Bragg wavelength, which are not phase matched, are essentially transparent. Therefore, light propagates through the grating with negligible attenuation or signal variation. Only those wavelengths that satisfy the Bragg condition are affected and strongly back-reflected. The ability to accurately preset and maintain the grating wavelength is a fundamental feature and advantage of fibre Bragg gratings.

The central wavelength of the reflected component satisfies the Bragg relation $\lambda_{Bragg} = 2n\Lambda$, where n is the index of refraction and Λ is the period of the index of refraction variation of the FBG. Due to the temperature and strain dependence of the parameters n and Λ, the wavelength of the reflected component will also change as a function of temperature and/or strain. This dependency is well known and allows determining the temperature or strain from the reflected FBG wavelength. A change of strain $\Delta\varepsilon$ and temperature ΔT will cause a wavelength shift $\Delta\lambda_B$ as in Eq. 5

$$\Delta\lambda_B/\lambda_B = (1 - P_e)\,\Delta\varepsilon + (\alpha + \xi)\,\Delta T \tag{7.1}$$

where P_e, α, and ξ are the elastic-optical coefficient, thermal expansion coefficient, and thermal-optical coefficient of the optical fibre, respectively. Figure 7.1 shows an example of time history of Bragg wavelength shift from one sensor when subjected to the passage of a loaded iron ore train. Based on the number of axles, which is obtained by counting the total number of peaks in the Bragg wavelength shift signal, the vehicle type can be identified. Furthermore, the magnitude of the peaks changes depending on the axle load.

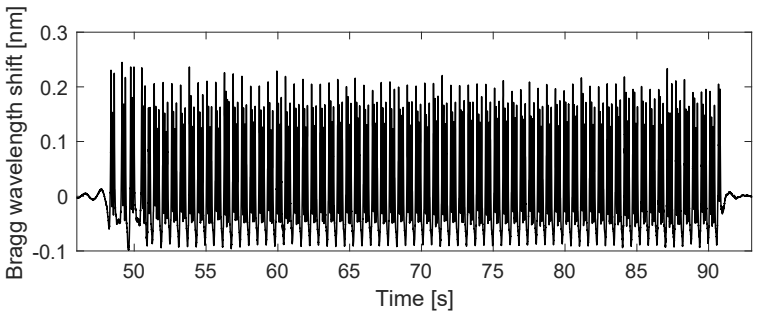

Figure 7.1. Time history of Bragg wavelength shift for a loaded iron ore train.

7.3 Instrumentation

In **Paper B**, the instrumentation set-up included sensors for the measurement of i) rail strains to assess rail bending moment and rail seat load; ii) vertical sleeper displacement; iii) vertical acceleration at sleeper end; iv) shear deformation of the rail to assess wheel load. An overview of the sensor positioning is shown in Figure 7.2. The setup included four clusters placed at sections between two sleepers in sleeper bays 3, 5, 8, and 11, numbered from the transition. Each FBG-based cluster comprised one accelerometer, one displacement transducer, and one strain array containing four strain gauges. One extra accelerometer was placed far from the transition, and another one on the first block on the slab side. Four temporary electrical strain gauge bridges were added to measure wheel–rail contact forces. The permanent installation of sensor clusters was used for condition monitoring of the transition. In contrast, the temporary installation was used to monitor dynamic wheel–rail contact forces for a single train. In total, 30 FBG sensors were installed. Aluminium covers were added to protect the sensors and cables from mechanical damage and the harsh weather conditions.

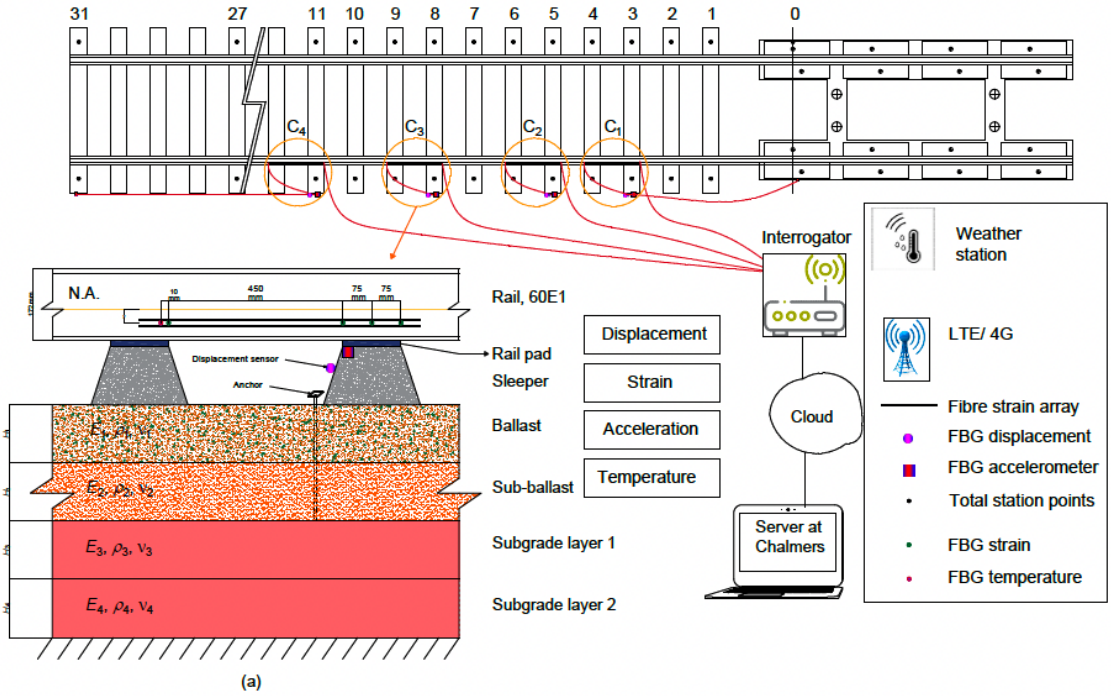

Figure 7.2. Schematic representation of the data acquisition system in the transition zone between ballasted track and 3MB slab track at Gransjö. The setup consists of four clusters (C1 – C4), each including a strain array (four strains on the rail web), a displacement transducer, and an accelerometer. From **Paper B**.

Each strain array was welded 31 mm below the neutral axis on one side of the rail to measure the magnitude of axial strain due to rail bending, as shown in Figures 7.3 and 7.4. The rail surface was polished and dried before the installation. Strain sensors 1, 2, and 3 in each cluster

were placed above a sleeper, while sensor 4 was located near the adjacent sleeper (see Figure 7.3). Due to the size of the displacement transducer and the limited available space, the transducer was positioned horizontally adjacent to the sleeper. Using a mechanism (L-shaped arm), the downward positive vertical displacement of the sleeper was converted to horizontal tension/compression of the displacement transducer, as shown in Figure 7.4. Further, vertical accelerations were measured using six FBG-based accelerometers. Five of these were placed at the ends of sleepers 3, 5, 8, 11, and 31, while one was positioned on the first block on the slab track side. Wheel–rail contact force is a primary indicator of dynamic vehicle–track interaction. In the current design for the monitoring setup, contact forces were considered complementary to the condition monitoring setup using the FBG sensors. In addition to the installed instrumentation, a track geometry recording car was used to measure vertical stiffness with a sampling distance of 5 cm along the slab and transition zone, as well as to serve as a quality controller for the longitudinal level of the track (not shown here). Further, the vertical settlement of several sleepers and the first block on the slab side were measured on several occasions using a total station. Examples of results from the measurements will be presented in the sections below.

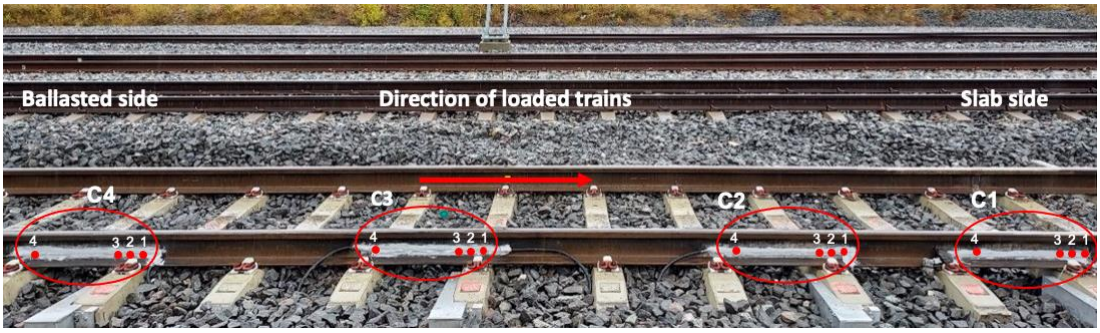

Figure 7.3. An overview of the four clusters (C1 – C4), and strain sensor numbering for each cluster.

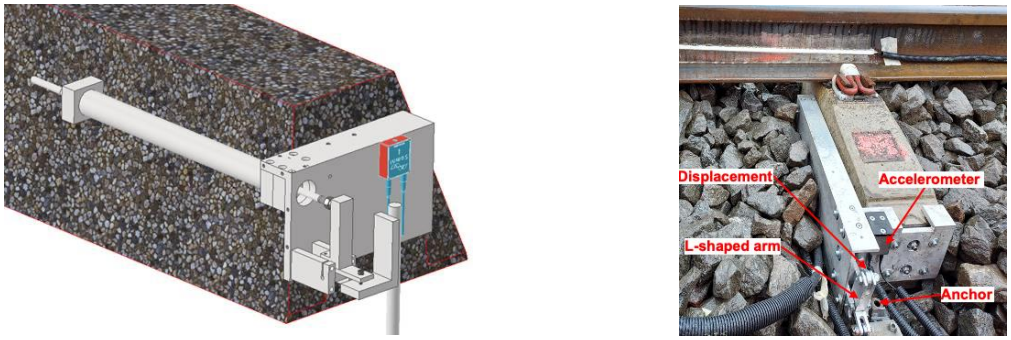

(a) (b)

Figure 7.4. Detail of sleeper containing a vertical base plate, an L-shaped mechanism, one accelerometer, and one displacement transducer. (a) The designed setup, (b) overview of an instrumented sleeper with an accelerometer and a displacement transducer. The positions of the anchor tip and the L-shaped mechanism are shown.

7.3.1 Rail strain and rail bending moment

Surface strain in a specimen can be measured by bonding an optical fibre with a fibre Bragg grating onto its surface. This requires a smooth and clean surface for effective adhesion. However, similar to measurements obtained using a single electrical strain gauge, this method does not allow for the separation of mechanically and thermally induced strains. Consequently, most FBG-based strain sensors have multiple gratings, i.e., one for strain sensing and one for temperature compensation. These sensors are packaged in a metal casing. They can be directly mounted on the specimen by a fastener, spot welding, or epoxy, which makes fibre handling easier and the sensor installation faster and more repeatable.

In the applied setup, strain and temperature were recorded in independent gratings. During a single train passage, the temperature variation was compensated. Further, it can be argued that the applied data sampling (2 kHz) is higher than the frequency range of interest for the quasi-static rail bending due to the train loads and speeds in this trial [133]. The strain signals were high-pass filtered at 1 Hz to adjust the baseline of the signal and prevent low-frequency drift. The signals were also detrended. In Figure 7.5, an example of rail strain above sleeper 11 due to the passing of a loaded iron ore train is depicted. By assuming Euler-Bernoulli beam theory for a known rail cross-section, and applying several sensors, the distribution of rail bending moment $M(x) = EI\varepsilon(x)$ along the rail can be determined. For example, based on three sensors, time histories of the distribution of rail bending moment on top of four sleepers along the transition due to a loaded iron ore train are presented in Figure 7.6. This information can be used to detect the type of vehicle, train speed, and as an indication of the track support condition.

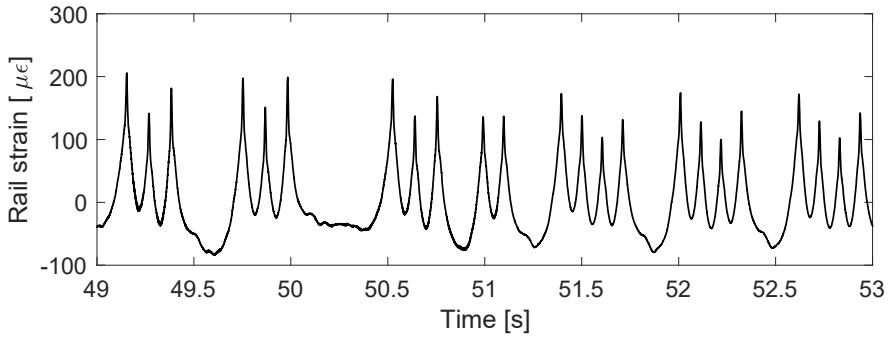

Figure 7.5. Time history of high-pass filtered (1 Hz) rail strain above sleeper 11 for part of a loaded iron ore train.

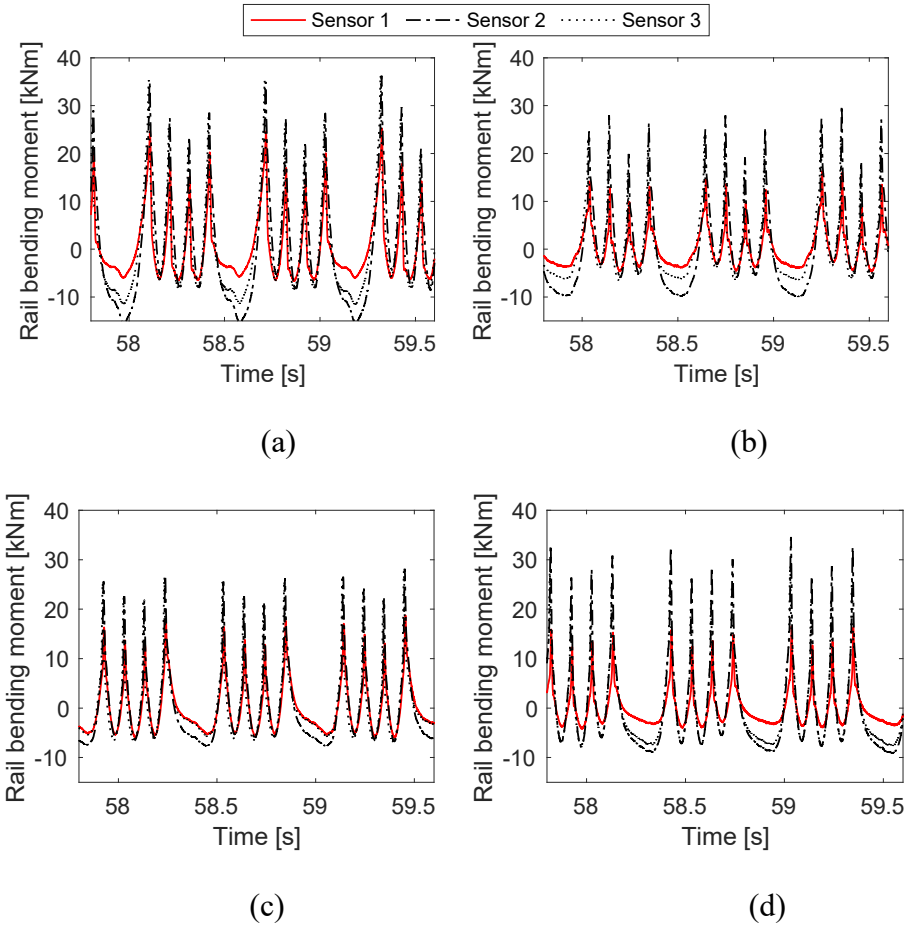

Figure 7.6. Time histories of rail bending moment above four sleepers along the transition due to part of a loaded iron ore train. (a) Sleeper 3, (b) sleeper 5, (c) sleeper 8, (d) sleeper 11. The loaded iron ore trains first pass over sensor 3, and then 2 and 1. From **Paper B**.

7.3.2 Vertical sleeper displacement and acceleration

In **Paper B**, a 4th-order low-pass Butterworth filter with a corner frequency of 30 Hz was applied to remove frequencies above those that dominated the track bed movement. While the frequencies of interest may be up to about 30 Hz, data must be acquired at much greater acquisition rates (here 2 kHz) to aid processing and eliminate noise and aliasing [134]. The zero-phase digital filtering, as implemented by *filtfilt* in Matlab, was applied to preserve the phase shift in the signal. One example of sleeper displacement is presented in Figure 7.7. In this study, the recorded acceleration signals were high-pass filtered at a cut-off frequency of 1 Hz, based on recommendations from the sensor provider. Unfortunately, it was found that the signal-to-noise ratio in the measured acceleration on the sleepers was too low to obtain reasonable data for sleeper displacement reconstruction. However, this was not the case for the acceleration signal on the 3MB slab track side due to the higher mass of the slab track. In

Figure 7.8, an example of a signal from the accelerometer on the first block, located on the slab track side, is depicted.

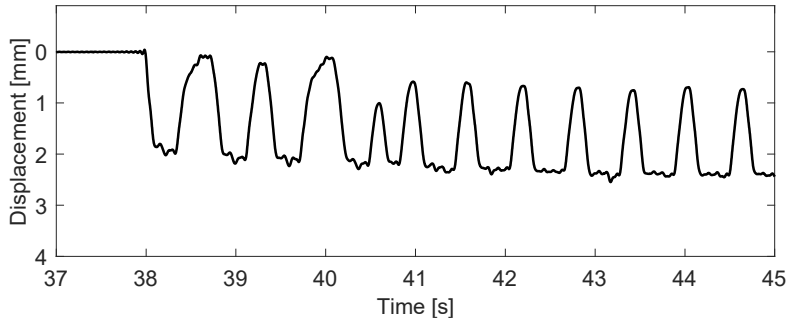

Figure 7.7. Time history of sleeper displacement signal from sleeper 11 for part of a loaded iron ore train. Displacement is presented relative to the displacement before the first axle in the first locomotive. Measurement from 2022-11-13.

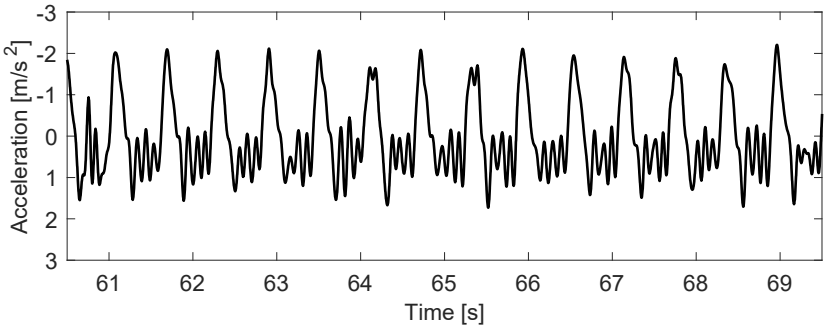

Figure 7.8. Time history of the sleeper acceleration signal from the first block on the slab track side for part of a loaded iron ore train. The signal has been band-pass filtered with cut-off frequencies at 1 and 30 Hz. Measurement from 2022-11-13.

7.3.3 Wheel–rail contact force

The vertical dynamic wheel–rail contact force was measured in three sleeper bays using a standard configuration with two pairs of strain gauges mounted on the rail web at the neutral axis, as shown in Figure 7.9. A half-bridge containing two waterproof strain gauges with a sensing area of 6 mm × 2.2 mm were glued on the neutral axis of the rail within a given span between two consecutive sleepers and oriented at ±45° with respect to the axes of the horizontal and vertical coordinate system. Two extra half bridges were glued to the other side of the rail in sleeper bay number 3 to study any effects of transverse offset in the wheel load. A data logger equipped with full-bridge completion modules was used to sample the strain gauges at a rate of 10 kHz. Examples of results from the contact force measurement are presented in **Paper B**. The measured wheel–rail contact forces showed notable variation in magnitude across different

spans. This variability may have been attributed to in-situ differences in support conditions from one sleeper to the next, whereas the simulations assumed a uniform foundation.

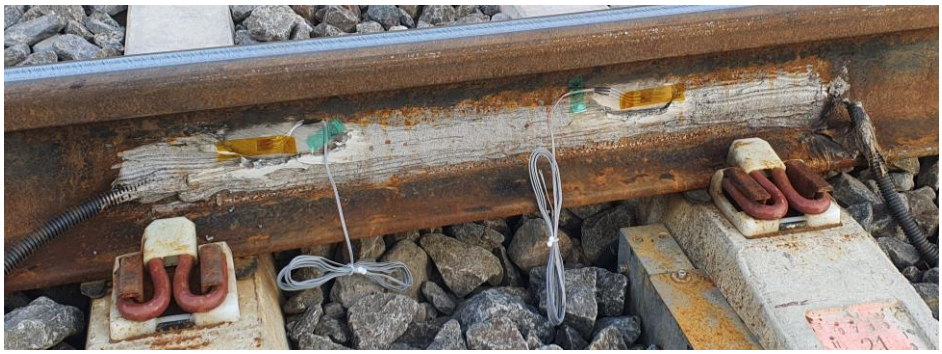

Figure 7.9. Full Wheatstone bridge mounted on the neutral axis of the rail web.

7.3.4 Long-term settlement

Permanent displacements of the track structure were determined by extracting the at-rest positions of the instrumented sleepers from intervals between train passages. Figure 7.10 presents the measured long-term track settlements for sleepers 5 and 11, alongside predictions from the 2D and 3D models described in **Paper C**. These results span approximately 11 months, including one winter season.

It is observed that the initial settlement rate immediately after the installation of the slab track and transition zone was very high, but it slowed down after a few weeks of traffic. For sleeper 11, there was a reversal in the permanent displacement during the winter due to frost heave. Due to the stiffness gradient and the evolving misalignment in rail level, there is a dynamic excitation of the vehicle–track system leading to a local maximum in settlement around sleepers 4 – 11 (at 2 – 6 m from the transition). This will create a loop of increasing dynamic excitation of the system, leading to higher sleeper–ballast contact forces, further settlement, etc. Note that the development of voided sleepers near the transition leads to a redistribution of load to adjacent sleepers farther away from the transition. This will generate higher settlements at these sleepers, and eventually a gradual shift in the location of the local maximum in longitudinal level. With reference to the empirical settlement model applied for the ballast layer in this thesis, it may be argued that due to the increase (hardening) of the settlement threshold value with increasing accumulated settlement, there is eventually a stabilisation (slowing down) of the settlement.

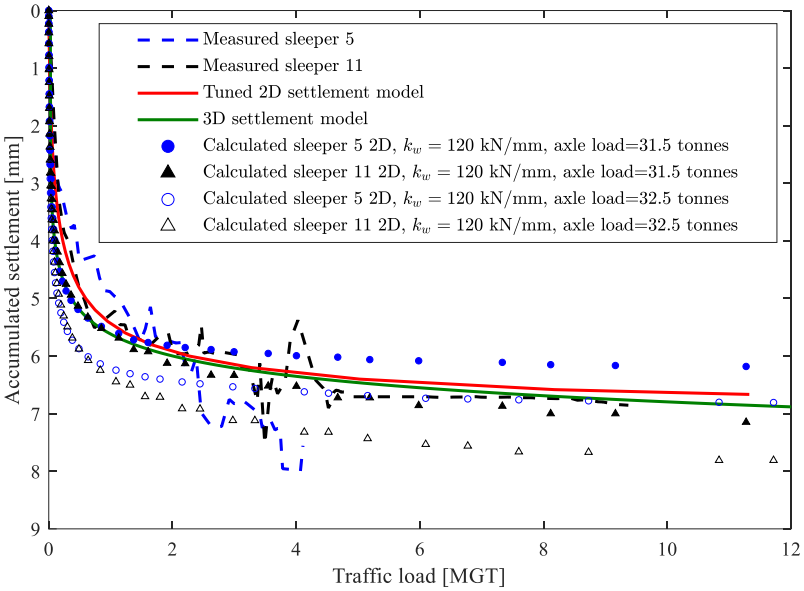

Figure. 7.10. Comparison of measured [9] and calculated accumulated settlements for sleepers 5 and 11. From **Paper B**.

7.3.5 Total station

A survey of sleeper levels was carried out using a Trimble S9 self-levelling, automatic tracking total station and active prism. The prism was placed in line with markings on each sleeper, and the total station was used to track and record the coordinates and height of the prism as it was moved sequentially from sleeper to sleeper along the track. The total station had an angular accuracy of 1 mm. Results from the total station survey are presented in **Paper B**.

The settlement of the 3MB system was thoroughly monitored by measuring the rail level using a total station along the 3MB slab on nine occasions over ten months, as shown in Figure 7.11. The surveys were conducted on September 15th (immediately after construction and before the first train passage), September 15th (after the first train passage), September 19th, September 20th, October 5th (post-tamping maintenance on the ballasted side and adding shims on the slab side), October 10th, October 27th, November 30th, February 9th, and April 21st. Figure 7.11 shows measured unloaded sleeper end settlement based on repeated total station surveys along 20 m of ballasted track (31 sleepers) after tamping. The data is presented relative to the measurement on October 10, 2022. The rail level was sampled at a distance of 8 m. After just two weeks of operation, the 3MB system had settled around 20 mm. A tamping maintenance procedure was performed to address this substantial settlement. This procedure restored the ballast's level on the ballasted side. Furthermore, shims were added at the two ends of the 3MB system to correct the dips identified at the slab system ends.

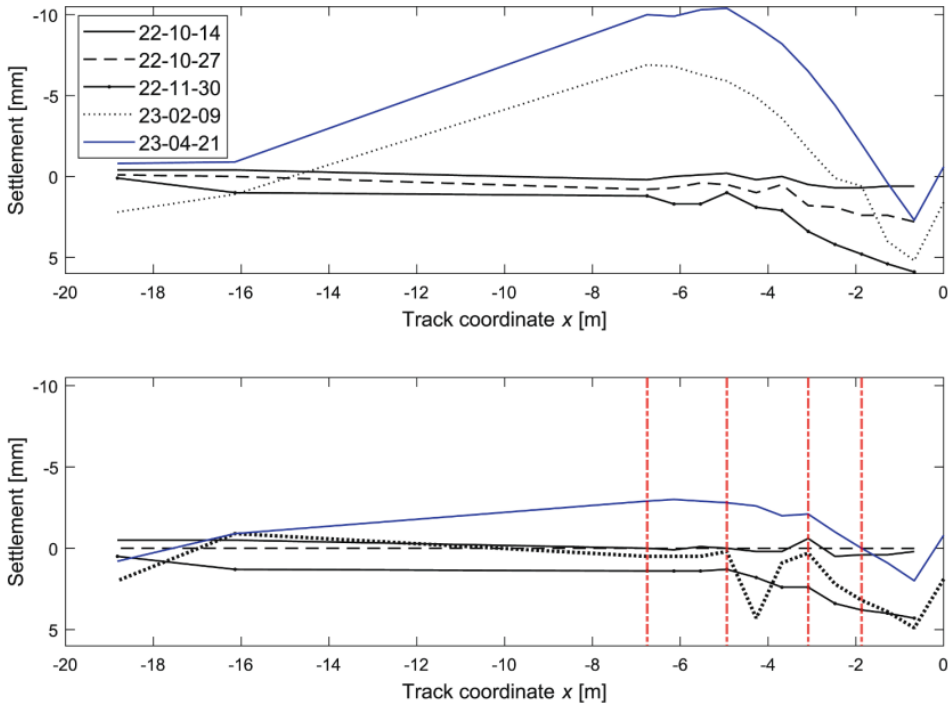

Figure 7.11. Measured unloaded sleeper end settlement based on repeated total station surveys along 20 m of ballasted track (31 sleepers). Data is presented relative to the measurement on October 10th, 2022. (a) Field side of the track where the sensor clusters were installed, (b) track side. The data for position $x = 0$ m corresponds to the measurement position on the first block in the slab track. The red vertical dashed lines show (from right) the positions of sleepers 3, 5, 8, and 11.

7.3.6 InSAR data and temperature

To evaluate the average long-term settlement at the test site, InSAR data was used, providing the average settlement over a specified surface area at various times. The mean settlement at a track point near the test site was found to be approximately 1 – 2 millimetres per year (**Paper C**), as illustrated in Figure 7.12. Additionally, it is observed that during the winter months, the track exhibits an upward trend rather than a decline in depth.

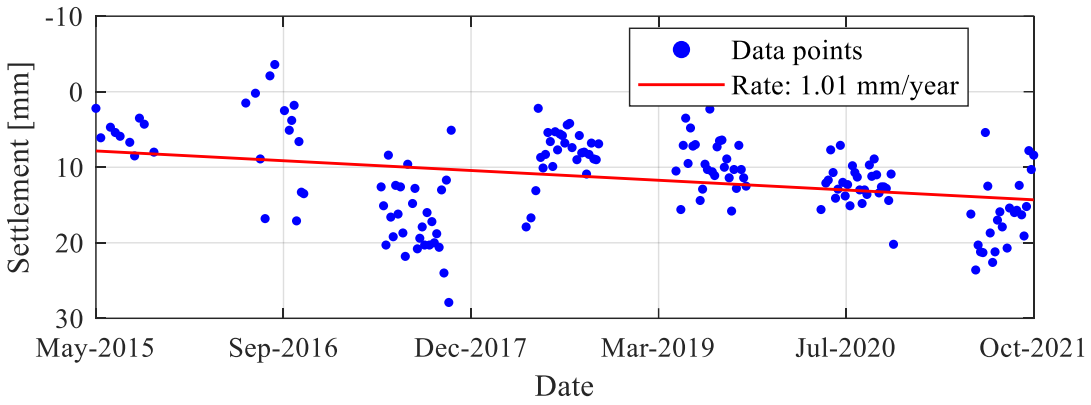

Figure 7.12. An example of InSAR long-term settlement measurements at a track point near the Gransjö site, covering the period from 2015 to 2021. Positive settlement numbers indicate downward permanent displacement. From **Papers B** and **C.**

7.3.7 Geotechnical investigation

Prior to the construction of the 3MB track, geotechnical investigations, including Cone Penetration Testing (CPT) and Multichannel Analysis of Surface Waves (MASW), were conducted to determine the stiffness and stratification of the layered substructure. The results indicated that the subgrade at the site consists almost entirely of moraine, interspersed with large blocks of rock, with bedrock located at a maximum depth of approximately 5 metres. The embankment height ranges from 2 to 2.5 m. Due to years of maintenance involving tamping and re-ballasting of the track, the thickness of the ballast layer (nominally 30 cm) has increased to 80 cm. In the MASW survey, the dispersion of Rayleigh waves on the ground surface, acquired using vertical geophones, was used for the interpretation of small-strain shear stiffness. See Figure 7.13 for an example of the measured distribution of wave speed in a cross-section of the subgrade at the test site.

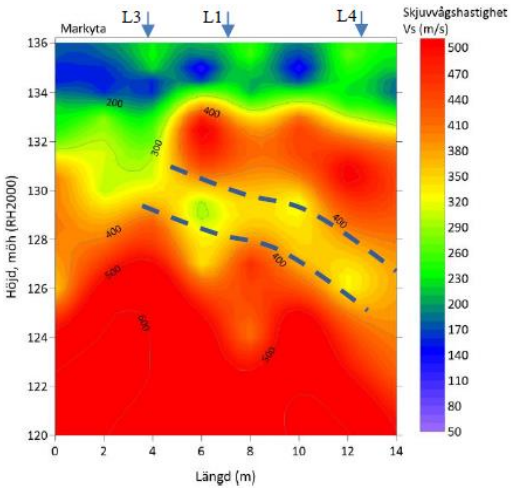

Figure 7.13. An example of the measured shear wave speed distribution of layered soil at the test site.

7.3.8 Track receptance

Vertical point and cross receptances (frequency response functions) of both track forms were measured by exciting the rail using an instrumented impact hammer and recording the track response with accelerometers. The rail was excited either above a rail seat or at the centre of a sleeper bay. Apart from the hammer excitation, the track was in unloaded conditions. For the ballasted track, see Figure 7.14, three resonance peaks can be observed in the measured receptance at 30, 290, and 950 Hz. The first peak corresponds to a vertical in-phase vibration of the rail and sleepers, characterised by high damping due to the propagation of waves in the ballast and subgrade. The second peak corresponds to an out-of-phase motion between the rail and sleepers, influenced by the flexibility of the rail pads. The third peak represents the pinned-pinned resonance mode, which is a vertical bending mode with a wavelength twice the sleeper span. Later, these responses were used to calibrate input data for the models in **Paper D**.

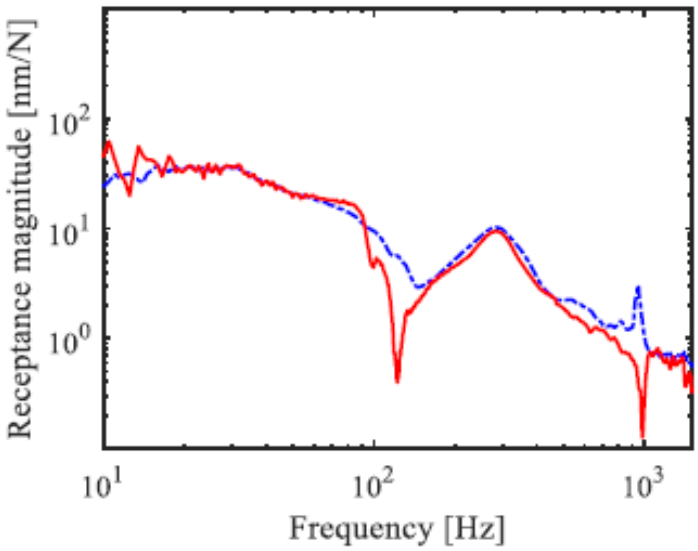

Figure 7.14. Magnitudes of measured rail receptances for the ballasted track. Vertical hammer excitation on the rail at midspan. Response measured on the rail at midspan (point receptance shown using a blue line) or on the rail at rail seat (cross receptance shown using a red line).

7.3.9 Track geometry cars

Track stiffness at rail level, measured using a track geometry recording car before and after construction of the 3MB track, is presented in Figure 7.15. A significant gradient in stiffness is observed at either end of the 48 m slab track. The mean value of the track stiffness is particularly low for the slab track due to the softer elastic pads and the poor compaction of the backfill material after the excavation carried out during construction.

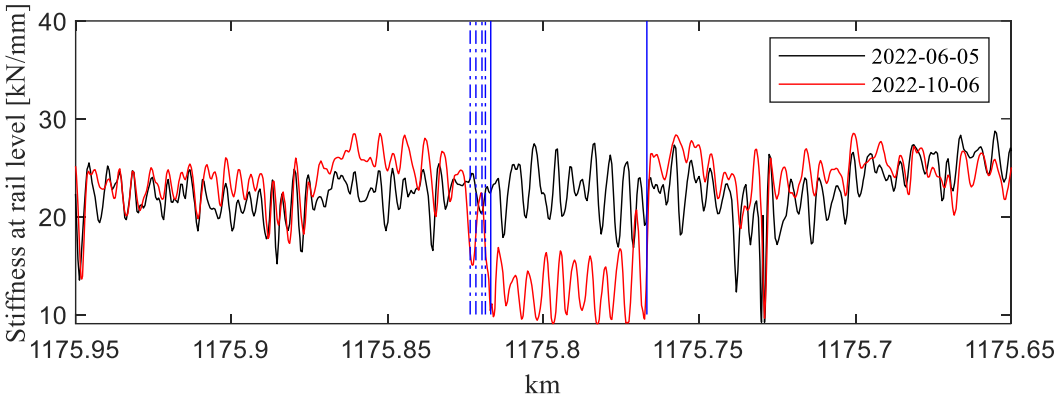

Figure 7.15. Track stiffness at rail level for ballasted track on embankment, two transition zones, and 48 m of slab track at Gransjö, measured by a track geometry recording car before and after construction. Blue vertical solid lines indicate the positions of two transitions (slab ends). Blue vertical dashed-dotted lines show the positions of instrumented sleepers 3, 5, 8, and 11, numbered from the slab.

8 Outline of the appended papers

Paper A: Prediction of long-term differential track settlement in a transition zone using an iterative approach

A methodology is presented for simulating long-term differential track settlement, the development of voided sleepers, and the evolution of vertical track irregularities at the transition between a ballasted track and a 3MB slab track. For a prescribed traffic load, the accumulated settlement is predicted using an iterative approach. It is based on a time-domain model of vertical dynamic vehicle–track interaction to calculate the contact forces between sleepers and ballast in the short term. These are used in an empirical model to determine the long-term settlement of the ballast/subgrade below each sleeper. The simulation procedure has been applied to the transition zone at Gransjö under heavy haul traffic, demonstrating its effectiveness in evaluating the influence of higher axle loads and the implementation of USPs. It is shown that the distribution of forces transmitted to the ballast varies along a transition zone. This is due to the stiffness gradient at the transition, but even more so when there is a misalignment in vertical rail level, for example, due to densification of ballast after the first few load cycles. In both cases, a transient pitching motion of the passing vehicles is generated, contributing to the dynamic loading and resulting in a local maximum in settlement at the sleepers a few metres from the transition. The use of USPs reduces track stiffness at the rail level, resulting in a more uniform distribution of load and reduced settlement along the track.

Paper B: Towards real-time condition monitoring of a transition zone in a railway structure using fibre Bragg grating sensors

An FBG-based setup for in-situ, long-term condition monitoring of track bed degradation in a transition zone has been developed and implemented to support the verification and calibration of the simulation model in **Paper A**. The system is designed for measurements on an operational railway track in harsh environmental conditions in northern Sweden. The instrumentation along the transition includes four clusters, each with an optical strain gauge array on the rail web in one sleeper bay, and an accelerometer and a displacement transducer on the sleeper. Complementary measurements were also conducted, including wheel–rail contact forces in selected sleeper bays using temporary electrical strain gauges, track stiffness at rail level assessed by track geometry cars, and rail receptance evaluated using hammer excitation tests. The results demonstrate that the implemented displacement and strain sensors effectively capture the full dynamic range of the system, indicating that the collected data accurately reflects the dynamic response of the transition zone in both the short term and long term, making them suitable for simulation model calibration.

Paper C: A review of methods and challenges for monitoring of differential settlement in railway transition zones

A review of methods for monitoring differential settlement in railway tracks is presented, along with recommendations for various aspects of condition monitoring. To measure the properties and loading of the superstructure, potential methods include FBG sensors, point track

receptance measurements, track geometry recording cars, and wheel impact load detectors (WILD). Subgrade characterisation can be carried out using techniques such as MASW, CPT, InSAR, frost sticks for temperature monitoring, and total stations. Lessons are learned from an in-situ measurement campaign involving an extensive FBG-based system, as described in **Paper B**. Integrating a combination of monitoring methods with a simulation model provides a robust framework for verifying and improving the accuracy of differential settlement predictions. This integrated approach is particularly effective in addressing challenges associated with track stiffness gradients and supports the development of improved transition zone designs.

Paper D: Benchmark of calibrated 2D and 3D track models for simulation of differential settlement in a transition zone using field measurement data

Two models for time-domain simulation of vertical dynamic vehicle–track interaction and the prediction of differential settlement in a transition zone between a ballasted track and a 3MB slab track are calibrated and verified using the field measurements described in **Paper B**. The model presented in **Paper A** is extended to include sleeper coupling through the ground, represented by a discretised mass-spring-damper system. The more detailed 3D model incorporates a solid representation of the layered soil foundation, with material properties derived from **Paper B** and absorbing boundaries applied to minimise wave reflections. Both models are used to simulate the passage of an iron ore freight vehicle through the transition zone. The accumulated settlement over one year of traffic is predicted using an iterative method and compared with the measured long-term sleeper settlement from **Paper B**. The results show good agreement between the simulations and field measurements, with the 2D model offering a significant computational advantage, requiring approximately 25 times less simulation time than the 3D model. An important finding is that results from the 3D model and field experiments indicate that an improved 2D model is needed to simulate long-term differential settlement efficiently.

Paper E: Influence of sleeper base area and spacing on long-term differential settlement in a railway track transition zone

The influence of adopting shorter sleeper spacing or a broader sleeper-base design for a given number of sleepers, aimed at reducing the track stiffness gradient between two track forms and thereby enhancing the dynamic vehicle–track interaction, is evaluated using the calibrated 2D track model presented in **Paper D**. The vehicle model represents a heavy-haul wagon with an axle load of 30 tonnes, operating at a speed of 60 km/h. The results indicate that implementing these design modifications reduces dynamic loading and contributes to enhanced long-term performance of the transition zone.

Paper F: Enhanced three-dimensional reduced-order track model for predicting differential settlement in railway transition zones

The models presented in **Papers A, D**, and **E** are further extended to incorporate additional static and dynamic influences of the soil, thereby enabling the simulation of transition designs implemented in the subgrade. The enhanced model combines a 2D vehicle model, a 3D nonlinear FE model of the track superstructure, and a linear 3D FE model of the layered subgrade. Mitigation measures in the subgrade to reduce the stiffness gradient at the transition between the two track forms are incorporated. The sleepers are represented by Euler–Bernoulli beam finite elements. To improve computational efficiency, the subgrade model is simplified using static condensation, resulting in a ROM. This methodology is applied to simulate differential settlement in transition zones between ballasted track on embankments and slab track on bridges or in tunnels. Each iteration involves a short-term analysis of the contact pressure at each sleeper–ballast interface to predict increments in ballast settlement and strains to calculate increments in permanent displacement within the subgrade layers. The iterative process continues until the prescribed traffic load is reached, yielding predictions of long-term settlement. The methodology is demonstrated by investigating the effects of implementing a transition wedge on the ballasted (softer) track side or softer rail pads on the (stiffer) slab track. Both directions of vehicle travel are considered.

Paper G: Dynamic vehicle-track interaction and differential settlement in a transition zone on railway ballast - An integrated 3D discrete-continuum model

A numerical method is presented for simulating the initial phase of differential settlement, considering the interaction effects among all components (i.e., rail, sleeper, ballast, and subballast particles) in a railway transition zone, using an integrated discrete–continuum approach. The method couples the DEM, the Finite Difference Method (FDM), and the FE model from **Paper A** to simulate vertical dynamic vehicle–track interaction within the transition zone. The 3D DEM model captures the discrete granular behaviour of the ballast and sub-ballast layers, while the continuum-based FDM model is used to represent the rail structure and the subgrade layer. Based on a time-domain model of vertical dynamic vehicle–track interaction, the nonlinear 2D FEM model, combined with an MBS model of the vehicle, calculates the contact forces between wheels and rails. These forces are then input into the DEM–FDM simulation to assess the non-uniform permanent displacements that develop within the granular layers. The support stiffness for each sleeper, used as input in the FEM model, is precomputed during the DEM–FDM coupling stage by applying a static load to each sleeper and calculating the resulting displacement. This methodology effectively simulates the gradual formation of voids beneath the sleepers, the redistribution of sleeper–ballast contact forces among adjacent sleepers, and the progressive development of vertical track irregularities due to accumulated traffic loading. The approach is demonstrated for a transition zone with a stiffness gradient between a softer ballast track and a stiffer track form, with accumulated settlements calculated after 500 axle passages.

9 Contributions of the thesis

This thesis advances the methodology for simulating and assessing vertical dynamic vehicle–track interaction and long-term differential settlement in railway transition zones. The key contributions are as follows:

Track and vehicle model development

- A 2D model of 3MB slab track and its transition to ballasted track (**Paper A**).
- Extension of the 2D track model to include sleeper coupling through the ground (**Paper D**).
- A detailed 3D transition zone model, incorporating static variation in stiffness of the layered soil foundation, coupled with the superstructure model (**Paper F**).
- Interaction between different components (i.e., rail, sleepers, and the ballast and sub-ballast layers), as well as between individual particles within the ballast and sub-ballast layers (**Paper G**).
- Application of dynamic loads from MBS simulations and consideration of particle rearrangement for ballast particles in the DEM model (**Paper G**).
- A 2D model of an iron ore vehicle, validated against a more comprehensive 3D model in the commercial software GENSYS (**Paper A**).

Foundation modelling enhancements

- Integration of static and dynamic foundation behaviour in the transition zone model:
  - Analytical approaches (**Paper A**).
  - Ballast masses, and shear coupling between adjacent sleepers using springs and dampers (**Paper D**).
  - Reduced-order model of layered soil (**Paper F**).
  - The ballast and sub-ballast are modelled as DEM and subgrade as FDM layers (**Paper G**).

Empirical settlement model improvements

- Development and calibration of an empirical settlement threshold model for ballast (**Papers A**, **C–F**).
- Implementation of an existing empirical model for soft subgrade layers (**Paper F**).
- Direct calculation of settlement without relying on empirical settlement models (**Paper G**).

Long-term settlement simulation framework

- Development of an iterative framework for simulating long-term differential settlement, voided sleeper formation, and evolving vertical track irregularities (**Papers A**, **C–F**).

Field measurement campaign

- Planning, development, and implementation of an in-situ measurement campaign in a transition zone (**Paper B**).

- Calibration and validation of simulation models using field data (**Papers B–D**).

Model benchmarking

- Benchmarking of calibrated 2D and 3D FE track models for simulation of differential settlement in transition zones (**Paper D**).

Design evaluation

- Assessment of various transition zone designs and their impact on wheel–rail contact forces, contact pressure on foundation surface, and long-term differential settlement:
  - USPs in **Paper A**.
  - Reduced sleeper spacing and wider sleeper base in **Paper D**.
  - Transition wedge and softer rail pads in **Paper F**.

Parametric studies

- Investigation of the effects of axle load, soil stiffness and damping, train speed, traffic direction, and longitudinal level irregularities on key track responses (**Papers A, D, F,** and **G**).

Loading

- Loads from the vehicle, including static axle loads, dynamic loads generated by low-frequency pitching motions in the bogies and carbody, and gravity loads (**Papers A-G**).

10 Conclusions

This thesis combines numerical modelling and field monitoring to investigate the short- and long-term behaviour of railway transition zones, with particular emphasis on the ballast–slab or tunnel transition. As part of this work, models of increasing fidelity have been developed and benchmarked against field data, enabling a more detailed study of the underlying engineering challenges. The findings provide valuable insights into the performance of transition zones over different timescales and demonstrate the effectiveness of various modelling approaches and mitigation strategies. Some of the significant findings include:

- A comprehensive simulation framework is developed for predicting long-term differential settlement, integrating various 2D and 3D track models with empirical settlement models for both ballast and subgrade layers.
- A transient pitching motion of passing vehicles, induced by the stiffness gradient at the transition between the two track forms, contributes to increased dynamic loading. This results in elevated levels of settlement at sleepers near the transition, where sleeper–ballast contact forces exceed the threshold defined in the empirical settlement model.
- The influence of an initial misalignment in rail level at the transition, such as that caused by ballast densification after the first few load cycles, has a greater influence on differential settlement than the stiffness gradient alone.
- Fibre Bragg Grating sensors, operated at high sampling frequencies and incorporating a wider range of sensor types (beyond strain) at a reasonable cost, have been shown to be highly valuable for railway condition monitoring, particularly when installation windows are limited. For comprehensive monitoring, a combination of measurement techniques is recommended.
- Static contributions of layered soil play a critical role in long-term differential settlement in a transition zone on soft subgrade (the influence of dynamic contribution could be considered in future work)
- Softer rail pads, USPs, shorter sleeper spacing, wider sleeper bases, and transition wedges can be effective in improving dynamic responses and reducing long-term differential settlement.
- Reduced-order models of the substructure can enrich simpler models by incorporating sufficient detail while keeping the computational time reasonable.
- DEM simulations provide valuable insights into the mechanisms of particle rearrangement, wave propagation, and, to some extent, damping as a function of densification in the ballast and sub-ballast layers, thereby governing transition zone behaviour and design.

11 Future work

Ideas for future research to further improve the understanding and optimisation of railway transition zones are:

- Based on simulation and field data, improved guidelines for transition zone design.
- Based on the presented 3D track model with flexible sleepers and a reduced-order model for the substructure, other transition zone designs, such as auxiliary rails, SHIELD, V-TRAS, geogrids, and soil/ballast improvement, can be investigated in terms of their impact on dynamic responses and long-term differential settlement.
- The influence of incorporating auxiliary rails not only on the ballasted (softer) side but also extending them to the stiffer side, albeit using a non-uniform rail profile, could be investigated.
- The presented 3D track model can be further enhanced by incorporating soil dynamics through a parameterised layered soil model that accounts for varying soil properties, porosity, and water content. Using advanced constitutive formulations would enable a more accurate representation of soil behaviour, capturing key features such as non-linear stiffness (as a function of stress and strain amplitude) and cyclic degradation. This approach would facilitate the investigation of how different soil characteristics influence long-term differential settlement, while still maintaining reasonable simulation times.
- In this thesis, the settlement on the engineering structure side of the transition (slab, bridge, or tunnel) has been neglected. This assumption can be re-evaluated and considered in future work. The effects of soil–structure interaction and their influence on long-term differential settlement should be investigated.
- The load on the first sleeper on the stiffer side of the transition slab or engineering structure is higher than that on the surrounding sleepers. The structural design of this sleeper warrants further investigation.
- Emerging techniques, such as neural networks and data-driven models, could be explored as alternatives to traditional numerical solvers in time-domain simulations. Physics-informed machine learning approaches, combined with the presented track models, may be considered.
- The settlement models used in this thesis are empirical and based on curve fitting. Future research could focus on developing more physically based settlement models that incorporates specific soil properties. Such models would improve the predictive capability for transition zones under more general and variable ground and traffic conditions.
- A digital twin of a transition zone, combining numerical models with real-time monitoring data, can be developed to support infrastructure management at system level.
- In this thesis, the interaction between rail and bridge was simplified using spring elements because the focus was on predicting the settlement on the ballasted side. Future work should aim to develop more accurate models to predict the dynamic train–bridge interaction.
- Dynamic contributions of layered soil could be further investigated in predictions of long-term differential settlement in a transition zone.

References

[1] Aggestam E. Slab track optimisation considering dynamic train-track interaction. PhD thesis, Chalmers University of Technology, Gothenburg, Sweden, 2021.

[2] Zuada Coelho B, Hölscher P, Priest J, Powrie W, Barends F. An assessment of transition zone performance. Proceedings of the Institution of Mechanical Engineers, Part F: Journal of Rail and Rapid Transit 2011;225:129–39.

[3] Ramos A, Gomes Correia A, Calçada R, Connolly DP. Ballastless railway track transition zones: an embankment to tunnel analysis. Transportation Geotechnics 2022; 33:100728.

[4] Indraratna B, Babar Sajjad M, Ngo T, Gomes Correia A, Kelly R. Improved performance of ballasted tracks at transition zones: a review of experimental and modelling approaches. Transportation Geotechnics 2019; 21:100260.

[5] Wang H, Markine V. Modelling of the long-term behaviour of transition zones: prediction of track settlement. Engineering Structures 2018; 156:294–304.

[6] Shan Y, Zhou S, Wang B, Ho CL. Differential settlement prediction of ballasted tracks in bridge–embankment transition zones. Journal of Geotechnical and Geoenvironmental Engineering 2020; 146:1–18.

[7] Siahkouhi M, Rashidi M, Miri A, Ghiasi A, et al. Ballasted railway track–bridge transition zone monitoring methods: recent developments, challenges, and prospects. Transportation Geotechnics 2025; 151:1–18.

[8] Aggestam E and Nielsen JCO. Multi-objective optimisation of transition zones between slab track and ballasted track using a genetic algorithm. Journal of Sound and Vibration 2019; 446:91–112.

[9] Nasrollahi K, Dijkstra J, and Nielsen JCO. Towards real-time condition monitoring of a transition zone in a railway structure using fibre Bragg grating sensors. Transportation Geotechnics 2024; 44:101166.

[10] Nasrollahi K, Ramos A, Nielsen JCO, Dijkstra J, and Ekh M. Benchmark of calibrated 2D and 3D track models for simulation of differential settlement in a transition zone using field measurement data. Engineering Structures 2024; 316:118555.

[11] Nasrollahi K, Nielsen JCO, Aggestam E, Dijkstra J, Ekh M. Prediction of long-term differential track settlement in a transition zone using an iterative approach. Engineering Structures 2023; 283:115830.

[12] Varandas JN, Hölscher P, Silva MAG. Settlement of ballasted track under traffic loading: application to transition zones. Proceedings of the Institution of Mechanical Engineers, Part F: Journal of Rail and Rapid Transit 2014;228:242–59.

[13] Varandas JN, Zhang Y, Shi J, Davies S, Ferreira A. Differential settlements monitoring in railway transition zones using satellite-based remote sensing techniques. Computer-Aided Civil and Infrastructure Engineering 2025;1–21.

[14] Varandas JN, Paixão A, Tijera Á, Crespo-Chacón I, Estaire J, Fortunato E. Dynamic response of ballasted high-speed railways: insights from experimental measurements and 3D nonlinear numerical modelling. Transportation Geotechnics 2025;52.

[15] Grossoni I, Hawksbee S, Jorge P, Bezin Y, Magalhaes H. Prediction of track settlement at high-speed railway transitions between embankment and bridge in the proximity of a turnout. Transportation Geotechnics 2022; 37:100879.

[16] Chumyen P, Connolly DP, Woodward PK, Markine V. A comparison of earthwork designs for railway transition zones. Construction and Building Materials 2023; 395:132295.

[17] Punetha P, Nimbalkar S, Khabbaz H. Analytical evaluation of ballasted track substructure response under repeated train loads. International Journal of Geomechanics 2020;20:1–2.

[18] Heydari-Noghabi H, Varandas JN, Esmaeili M, Zakeri JA. Investigating the influence of auxiliary rails on dynamic behaviour of railway transition zone by a 3D train-track interaction model. Latin American Journal of Solids and Structures 2017; 14:2000–18.

[19] Stastny A, Medicus G, Galavi V, Tafili M, Tschuchnigg F. Evaluation of advanced soil models for the cyclic soil-structure interaction of integral bridges. Acta Geotechnica 2025;9.

[20] Barbosa JM de O, Fărăgău AB, van Dalen KN, Steenbergen MJMM. Modelling ballast via a non-linear lattice to assess its compaction behaviour at railway transition zones. Journal of Sound and Vibration 2022;530.

[21] Tutumluer E, Stark TD, Mishra D, Hyslip JP. Investigation and mitigation of differential movement at railway transitions for US high-speed passenger rail and joint passenger/freight corridors. Proceedings of the 2012 Joint Rail Conference (JRC 2012) 2012:75–84.

[22] Sañudo R, Cerrada M, Alonso B, Dell'Olio L. Analysis of the influence of support positions in transition zones: a numerical analysis. Construction and Building Materials 2017; 145:207–17.

[23] Jain A, Metrikine AV, Steenbergen MJMM, van Dalen KN. Design of railway transition zones: a novel energy-based criterion. Transportation Geotechnics 2024; 46:101223.

[24] Talebi N, Ahlström J, Ekh M, Meyer KA. Evaluations and enhancements of fatigue crack initiation criteria for steels subjected to large shear deformations. International Journal of Fatigue 2024;182.

[25] Kabo E, Ekberg A. Characterisation of track buckling resistance. Proceedings of the Institution of Mechanical Engineers, Part F: Journal of Rail and Rapid Transit 2024;238:786–94.

[26] Haghighi E, Kasraei A, Famurewa S, Strandberg G, Sas G, Garmabaki AHS. Climate change risks on railway infrastructure: a systematic review and analysis. Sustainable Cities and Society 2025;129.

[27] Karlsson R. Tekniska systemkrav för Ostlänken (technical system requirements for Ostlänken, in Swedish). Trafikverket; vol. 1v2.0. 2014.

[28] Shahraki M, Warnakulasooriya C, Witt KJ. Numerical study of transition zone between ballasted and ballastless railway track. Transportation Geotechnics 2015; 3:58–67.

[29] Selig ET, Waters JM. Track geotechnology and substructure management. London: Thomas Telford; 1994.

[30] Li D, Selig ET. Method for railroad track foundation design. II: applications. Journal of Geotechnical and Geoenvironmental Engineering 1998; 124:323–9.

[31] Dahlberg T. Some railroad settlement models: a critical review. Proceedings of the Institution of Mechanical Engineers, Part F: Journal of Rail and Rapid Transit 2001;215:289–300.

[32] Paixão A. Transition zones in railway tracks: an experimental and numerical study on the structural behaviour. PhD thesis. Faculty of Engineering, University of Porto, Porto, Portugal; 2014.

[33] Esveld C. Modern railway track. 2nd ed. Zaltbommel: MRT-Productions; 2001.

[34] Ahmadi A, Nasrollahi K, Nielsen JCO, Dijkstra J. Dynamic vehicle–track interaction and differential settlement in a transition zone on railway ballast: an integrated 3D discrete–continuum model. Submitted to International Journal of Geomechanics.

[35] Aela P, Powrie W, Harkness J, Jing G. Discrete element modelling of railway ballast problems: an overview. Dordrecht: Springer Netherlands; 2024.

[36] Froehlke C, Dersch M, Edwards R, Lima A de O, Tutumluer E. Effect of sub-freezing temperatures on ballast strength: a laboratory study. Transportation Geotechnics 2025; 52:101551.

[37] Li D, Hyslip J, Sussmann T, Chrismer S. Substructure. In: Railway geotechnics. Boca Raton: CRC Press; 2002.

[38] Aggestam E, Nielsen JCO. Simulation of vertical dynamic vehicle–track interaction using a three-dimensional slab track model. Engineering Structures 2020; 222:1633–57.

[39] Morales-Gamiz FJ. Design requirements, concepts, and prototype test results for new system of ballastless system (3MB slab track), Capacity for rail; Deliverable 11.3. 2017.

[40] Namura A, Suzuki T. Evaluation of countermeasures against differential settlement at track transitions. Quarterly Report of RTRI (Railway Technical Research Institute, Japan) 2007;48:176–82.

[41] Peduto D, Giangreco C, Venmans AAM. Differential settlements affecting transition zones between bridges and road embankments on soft soils: numerical analysis of maintenance scenarios by multi-source monitoring data assimilation. Transportation Geotechnics 2020;24:100369.

[42] Charoenwong C, Connolly DP, Woodward PK, Galvín P, and Alves Costa P. Numerical modelling of the evolution of differential settlement of railway tracks. Proceedings of the

11th International Conference on the Bearing Capacity of Roads, Railways and Airfields, Volume 3 2022;3:291–300.

[43] Nielsen JCO and Li X. Railway track geometry degradation due to differential settlement of ballast/subgrade: numerical prediction by an iterative procedure. Journal of Sound and Vibration 2018; 412:441–56.

[44] Li X, Ekh M, and Nielsen JCO. Three-dimensional modelling of differential railway track settlement using a cycle domain constitutive model. International Journal for Numerical and Analytical Methods in Geomechanics 2016; 40:1758–70.

[45] Guo Y and Zhai W. Long-term prediction of track geometry degradation in high-speed vehicle–ballastless track system due to differential subgrade settlement. Soil Dynamics and Earthquake Engineering 2018; 113:1–11.

[46] Nicks JE. The bump at the end of the railway bridge. PhD thesis. Texas A&M University, Texas, United States; 2009.

[47] Zaman BM, Gopalasingam A, and Laguros JG. Consolidation settlement of bridge approach foundation. Journal of Geotechnical Engineering 1991; 117:219–40.

[48] Long JH, Olson SM, Stark TD, and Samara EA. Differential movement at embankment–bridge structure interface in Illinois. Transportation Research Record 1998:53–60.

[49] Wheeler LN, Take WA, Hoult NA, Le H. Use of fibre optic sensing to measure distributed rail strains and determine rail seat forces under a moving train. Canadian Geotechnical Journal 2019; 56:1–13.

[50] Li M. Simulations of the vertical track stiffness and its variations for slab track along transition zones Simulations of the vertical track stiffness and its variations for slab track along transition zones 2018:1–51.

[51] Le Pen L, Milne D, Thompson D, and Powrie W. Evaluating railway track support stiffness from trackside measurements in the absence of wheel load data. Canadian Geotechnical Journal 2016; 53:1156–66.

[52] Dahlberg T. Railway track stiffness variations: consequences and countermeasures. International Journal of Civil Engineering 2010; 8:1–12.

[53] Nielsen J. Optimum vertical track stiffness. Research report 2010:11. Department of Applied Mechanics, Chalmers University of Technology, Gothenburg, Sweden; 2010.

[54] Oscarsson J. Dynamic train–track interaction: variability attributable to scatter in the track properties. Vehicle System Dynamics 2002; 37:59–79.

[55] Sañudo R, Dell'Olio L, Casado JA, Carrascal IA, and Diego S. Track transitions in railways: a review. Construction and Building Materials 2016; 112:140–57.

[56] Nasrollahi K and Nielsen J. Influence of sleeper base area and spacing on long-term differential settlement in a railway track transition zone. Proceedings of the Sixth International Conference on Railway Technology: Research, Development and Maintenance (Railway Technology 2024, 1–5 September 2024, Prague, Czech Republic). 2024;7:1–11.

[57] Chumyen P, Connolly DP, Woodward PK, and Markine V. The effect of soil improvement and auxiliary rails at railway track transition zones. Soil Dynamics and Earthquake Engineering 2022; 155:107200.

[58] Faragau AB, Jain A, de Oliveira Barbosa JM, and Metrikine AV, van Dalen KN. Auxiliary rails as a mitigation measure for degradation in transition zones. Proceedings of the Fifth International Conference on Railway Technology: Research, Development and Maintenance 2023;1:1–7.

[59] Paixão A, Varandas JN, Fortunato E, and Calçada R. Numerical simulations to improve the use of under sleeper pads at transition zones to railway bridges. Engineering Structures 2018; 164:169–82.

[60] Insa R, Salvador P, Inarejos J, Roda A. Analysis of the influence of under sleeper pads on the railway vehicle/track dynamic interaction in transition zones. Proceedings of the Institution of Mechanical Engineers, Part F: Journal of Rail and Rapid Transit 2012;226:409–20.

[61] Le Pen L, Watson G, Hudson A, Powrie W. Behaviour of under sleeper pads at switches and crossings: field measurements. Proceedings of the Institution of Mechanical Engineers, Part F: Journal of Rail and Rapid Transit 2018;232:1049–63.

[62] Sasaoka CD, Davis DD, Koch K, Reiff RP. Implementing track transition solutions. Technology Digest TD-05-001; 2005.

[63] Abadi T, Le Pen L, Zervos A, Powrie W. Effect of sleeper interventions on railway track performance. Journal of Geotechnical and Geoenvironmental Engineering 2019; 145:04019009.

[64] Xin T, Ding Y, Wang P, Gao L. Application of rubber mats in transition zone between two different slab tracks in high-speed railway. Construction and Building Materials 2020; 243:118219.

[65] Li H and McDowell GR. Discrete element modelling of under sleeper pads using a box test. Granular Matter 2018; 20:1–12.

[66] Insley PS. Self-compensating sleeper and method of maintaining a railroad track. Patent No. EP3608472A1; 2020.

[67] Jia W, Markine V, Carvalho M, Connolly DP, Guo Y. Design of a concept wedge-shaped self-levelling railway sleeper. Construction and Building Materials 2023; 386:131524.

[68] Puppala A, Saride S, Archeewa E, Hoyos L, Nazarian S. Recommendations for design, construction, and maintenance of bridge approach slabs: synthesis report. Technical report; 2009.

[69] Jing G, Qie L, Markine V, Jia W. Polyurethane reinforced ballasted track: review, innovation and challenge. Construction and Building Materials 2019; 208:734–48.

[70] Wu Y, Shi C, Yu Y, Chen H, Fan Y, Wang H, et al. Dynamic behaviour of precast epoxy asphalt track bed for transition zone in high-speed railway: a numerical approach. Transportation Geotechnics 2023; 40:100960.

[71] Sehgal L, Garg A, Sehgal V, Buttlar W. Hot mix asphalt in ballasted railway track: international experience and inferences. Proceedings of the Institution of Permanent Way Engineers (IPWE) International Technical Seminar 2017:1–12.

[72] Rose JG, Anderson JS. Long-term performance of asphalt underlayment trackbeds for special trackbed applications. Technical report; 2006:1–27.

[73] Jing G, Siahkouhi M, Wang H, Esmaeili M. The improvement of the dynamic behaviour of railway bridge transition zone using furnace slag reinforcement: a numerical and experimental study. Proceedings of the Institution of Mechanical Engineers, Part F: Journal of Rail and Rapid Transit 2022;236:362–74.

[74] Jain A, Marykovskiy Y, Metrikine AV, van Dalen KN. Quantifying the impact of stiffness distributions on the dynamic behaviour of railway transition zones. Transportation Geotechnics 2024; 45:101211.

[75] Fara A. Transition zones for railway bridges: a study of the Sikån bridge. Master's thesis. Department of Civil, Environmental, and Natural Resources Engineering, Luleå University of Technology, Luleå, Sweden; 2014.

[76] Li D, Davis D. Transition of railroad bridge approaches. Journal of Geotechnical and Geoenvironmental Engineering 2005; 131:1392–8.

[77] Lanca A, Dimitrovová Z, Barroso M, Fontul S. Numerical analysis of geogrid contribution to railway track reinforcement. MATEC Web of Conferences 2018; 211:1–6.

[78] Rose JG, Stark TD, Wilk ST, Purcell M. Design and monitoring of well-performing bridge transitions. Proceedings of the 2015 Joint Rail Conference (JRC 2015) 2015:1–9.

[79] Rhomberg Sersa Rail Group. V-tras UTM: Different CB. Rail Group Supplier of Complete Range of Railway Technologies.

[80] Wang H, Markine V. Corrective countermeasure for track transition zones in railways: adjustable fastener. Engineering Structures 2018; 169:1–14.

[81] Nielsen JCO, Igeland A. Vertical dynamic interaction between train and track: influence of wheel and track imperfections. Journal of Sound and Vibration 1995; 187:825–39.

[82] Lamprea-Pineda AC, Connolly DP, Hussein MFM. Beams on elastic foundations: a review of railway applications and solutions. Transportation Geotechnics 2022; 33:100696.

[83] Lei X, Mao L. Dynamic response analyses of vehicle and track coupled system on track transition of conventional high-speed railway. Journal of Sound and Vibration 2004; 271:1133–46.

[84] Ramos A, Gomes Correia A, Calçada R, Alves Costa P, Esen A, Woodward PK, et al. Influence of track foundation on the performance of ballast and concrete slab tracks under cyclic loading: physical modelling and numerical model calibration. Construction and Building Materials 2021; 277:122245.

[85] Dahal B, Mishra D. Discrete element modelling of permanent deformation accumulation in railroad ballast considering particle breakage. Frontiers in Built Environment 2020; 5:1–14.

[86] Chen C, McDowell GR. An investigation of the dynamic behaviour of track transition zones using discrete element modelling. Proceedings of the Institution of Mechanical Engineers, Part F: Journal of Rail and Rapid Transit 2016;230:117–28.

[87] Shi C, Zhao C, Zhang X, Andersson A. Analysis on dynamic performance of different track transition forms using the discrete element/finite difference hybrid method. Computers and Structures 2020; 230:106187.

[88] Liu Z, Li W, Shoemaker TA, Tutumluer E, Hashash YMA. Investigation of hanging crosstie problem at bridge approaches: a train–track–bridge model coupled with discrete element method. Railway Engineering Science 2025.

[89] Zuada Coelho B, Varandas JN, Hijma MP, Zoeteman A. Towards network assessment of permanent railway track deformation. Transportation Geotechnics 2021;29.

[90] Wolf JP, Deeks AJ. Foundation vibration analysis: a strength-of-materials approach. Amsterdam: Elsevier; 2004.

[91] Nielsen JCO. High-frequency vertical wheel–rail contact forces: validation of a prediction model by field testing. Wear 2008; 265:1465–71.

[92] Li D, Selig ET. Cumulative plastic deformation for fine-grained subgrade soils. Journal of Geotechnical Engineering 1996; 122:1006–13.

[93] Gazetas G. Foundation vibrations. Athens: National Technical University of Athens; 1991.

[94] Suiker ASJ, Selig ET, Frenkel R. Static and cyclic triaxial testing of ballast and sub-ballast. Journal of Geotechnical and Geoenvironmental Engineering 2005; 131:771–82.

[95] Shenton MJ. Deformation of railway ballast under repeated loading conditions. In: Railroad track mechanics and technology. New York: Pergamon; 1978. p. 405–25.

[96] Iwnicki S, Grassie S, Kik W. Track settlement prediction using computer simulation tools. Vehicle System Dynamics 2000;33:37–46.

[97] Abadi T, Le Pen L, Zervos A, Powrie W. A review and evaluation of ballast settlement models using results from the Southampton Railway Testing Facility (SRTF). Procedia Engineering 2016;143:999–1006.

[98] Rempelos G, Ognibene G, Le Pen L, Blainey S, Preston J, Powrie W. Railway track deterioration models: a review of the state of the art. Transportation Geotechnics 2024;49:10137

[99] Grossoni I, Powrie W, Zervos A, Bezin Y, Le Pen L. Modelling railway ballasted track settlement in vehicle–track interaction analysis. Transportation Geotechnics 2021;26:100433.

[100] Lakušić S, Ahac M, Haladin I. Experimental investigation of railway track with under sleeper pad. Proceedings of the 10th Slovenian Road and Transportation Congress 2010:386–93.

[101] Ng CWW, Zhou C, Yuan Q, Xu J. Resilient modulus of unsaturated subgrade soil: experimental and theoretical investigations. Canadian Geotechnical Journal 2013; 50:223–32.

[102] Li D, Selig ET. Resilient modulus for fine-grained subgrade soils. Journal of Geotechnical Engineering 1994; 120:939–57.

[103] Banimahd M. Advanced finite element modelling of coupled train–track systems: a geotechnical perspective. PhD thesis; 2008.

[104] Suiker ASJ, de Borst R. A numerical model for the cyclic deterioration of railway tracks. International Journal for Numerical Methods in Engineering 2003; 57:441–70.

[105] Sato Y. Japanese studies on deterioration of ballasted track. Vehicle System Dynamics 1995; 24:197–208.

[106] Ognibene G, Le Pen L, Harkness J, Zervos A, Powrie W. An alternative approach to track settlement prediction. Lecture Notes in Civil Engineering 2022; 165:99–112.

[107] Charoenwong C, Connolly DP, Woodward PK, Galvín P, Alves Costa P. Analytical forecasting of long-term railway track settlement. Computers and Geotechnics 2022; 143:104601.

[108] Peltomäki M, Kolisoja P, Luomala H. Novel permanent deformation model for granular materials. Transportation Geotechnics 2025;51.

[109] Sayeed MA, Shahin MA. Dynamic response analysis of ballasted railway track–ground system under train moving loads using 3D finite element numerical modelling. Transportation Infrastructure Geotechnology 2023; 10:639–59.

[110] Khajehei H, Ahmadi A, Soleimanmeigouni I, Haddadzade M, Nissen A, Latifi Jebelli MJ. Prediction of track geometry degradation using artificial neural network: a case study. International Journal of Rail Transportation 2022; 10:24–43.

[111] Soleimanmeigouni I, Ahmadi A, Kumar U. Track geometry degradation and maintenance modelling: a review. Proceedings of the Institution of Mechanical Engineers, Part F: Journal of Rail and Rapid Transit 2018;232:73–102.

[112] Ren J., Liu W., Du W., Zheng J., Wei H., Zhang K., et al. Identification method for subgrade settlement of ballastless track based on vehicle vibration signals and machine learning. Construction and Building Materials 2023; 369:130573.

[113] Guo Y, Zhai W. Long-term prediction of track geometry degradation in high-speed vehicle–ballastless track system due to differential subgrade settlement. Soil Dynamics and Earthquake Engineering 2018; 113:1–11.

[114] Xu W, Guo Y, You M. Intelligent identification of differential subgrade settlement of ballastless track system based on vehicle dynamic responses and 1D-CNN approach. Transportation Geotechnics 2024;48.

[115] Peng B, van Dalen KN, Li Z, Kaewenruen S, Xu L, Shiau J, et al. Spatial–temporal evolution prediction of train-induced settlement in railway transition zones using a simplified iterative approach. Journal of Sound and Vibration 2025:119360.

[116] Ramos A, Gomes Correia A, Nasrollahi K, Nielsen JCO, Calçada R. Machine learning models for predicting permanent deformation in railway tracks. Transportation Geotechnics 2024;47.

[117] Verruijt A. Theory and applications of transport in porous media: an introduction to soil mechanics. Cham: Springer; 2018.

[118] Powrie W, Yang LA, Clayton CRI. Stress changes in the ground below ballasted railway track during train passage. Proceedings of the Institution of Mechanical Engineers, Part F: Journal of Rail and Rapid Transit 2007;221:247–61.

[119] Timoshenko S, Goodier JN. Theory of elasticity. 2nd ed. New York: McGraw-Hill; 1951.

[120] Kouroussis G, Caucheteur C, Kinet D, Alexandrou G, Verlinden O, Moeyaert V. Review of trackside monitoring solutions: from strain gages to optical fibre sensors. Sensors 2015;15:20115–39.

[121] Rahman MA, Taheri H, Dababneh F, Karganroudi SS, Arhamnamazi S. A review of distributed acoustic sensing applications for railroad condition monitoring. Mechanical Systems and Signal Processing 2024;208.

[122] Berggren E. Railway track stiffness: dynamic measurements and evaluation for efficient maintenance. PhD thesis. KTH Royal Institute of Technology, Stockholm, Sweden; 2009.

[123] Luomala H. Monitoring the vertical deformation behaviour of road and railway structures. PhD thesis. Tampere University, Finland; 2019.

[124] Wang H, Markine V, Liu X. Experimental analysis of railway track settlement in transition zones. Proceedings of the Institution of Mechanical Engineers, Part F: Journal of Rail and Rapid Transit 2018;232:1774–89.

[125] Milne D, Harkness J, Le Pen L, Powrie W. The influence of variation in track level and support system stiffness over longer lengths of track for track performance and vehicle track interaction. Vehicle System Dynamics 2021;59:245–68.

[126] Wheeler LN, Pannese E, Hoult NA, Take WA, Le H. Measurement of distributed dynamic rail strains using a Rayleigh backscatter-based fiber optic sensor: lab and field evaluation. Transportation Geotechnics 2018;14:70–80.

[127] Stoura CD, Dertimanis VK, Hoelzl C, Kossmann C, Cigada A, Chatzi EN. A model-based Bayesian inference approach for on-board monitoring of rail roughness profiles: application on field measurement data of the Swiss Federal Railways network. Structural Control and Health Monitoring 2023;2023.

[128] Sauni M, Luomala H, Kolisoja P, Vaismaa K. Framework for implementing track deterioration analytics into railway asset management. Built Environment Project and Asset Management 2022;12:871–86.

[129] Berggren EG, Nissen A, Paulsson BS. Track deflection and stiffness measurements from a track recording car. Proceedings of the Institution of Mechanical Engineers, Part F: Journal of Rail and Rapid Transit 2014;228:570–80.

[130] Nielsen JCO, Berggren EG, Hammar A, Jansson F, Bolmsvik R. Degradation of railway track geometry: correlation between track stiffness gradient and differential settlement. Proceedings of the Institution of Mechanical Engineers, Part F: Journal of Rail and Rapid Transit 2020;234:108–19.

[131] Yan TH, Hoelzl C, Corman F, Dertimanis V, Chatzi E. Integration of on-board monitoring data into infrastructure management for effective decision-making in railway maintenance. Railway Engineering Science 2025.s

[132] Bernal E, Spiryagin M, Cole C. Onboard condition monitoring sensors, systems and techniques for freight railway vehicles: a review. IEEE Sensors Journal 2019;19:4–24.

[133] Thompson D. Railway noise and vibration: mechanisms, modelling and means of control. Southampton: University of Southampton; 2009.

[134] Powrie W, Le Pen L, Milne D, Watson G, Harkness J. Behaviour of under-track crossings on ballasted railways. Transportation Geotechnics 2019;21:100258.